

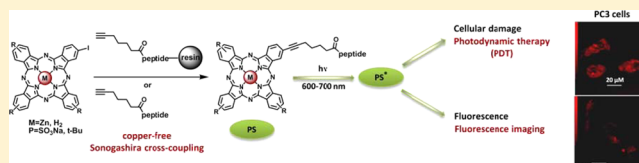
Phthalocyanine–Peptide Conjugates: Receptor-Targeting Bifunctional Agents for Imaging and Photodynamic Therapy

Elena Ranyuk,[†] Nicole Cauchon,[†] Klaus Klarskov,[‡] Brigitte Guérin,^{*,†} and Johan E. van Lier^{*,†}

[†]Department of Nuclear Medicine and Radiobiology and [‡]Department of Pharmacology Faculty of Medicine and Health Sciences, Université de Sherbrooke, Sherbrooke, Québec, Canada

S Supporting Information

ABSTRACT: The synthesis of a series of new zinc phthalocyanine–peptide conjugates targeting the gastrin-releasing peptide (GRP) and integrin receptors is reported. Two alternative synthetic methods based on Sonogashira cross-coupling of an iodinated zinc phthalocyanine with acetylenic bombesin or arginine–glycine–aspartic acid (RGD) derivatives, either in solution or on solid phase, are presented. The water-soluble conjugates were screened for their photodynamic efficacy against several cancer cell lines expressing different levels of GRP and integrin receptors, and their intracellular localization was evaluated via confocal fluorescence microscopy. Variations in photocytotoxicity between the conjugates correlate to differences in hydrophobicity as well as receptor-mediated cell uptake. In the case of the phthalocyanine–bombesin conjugate, competition experiments confirm the involvement of the GRP receptor in both the phototherapeutic activity as well as intracellular localization. These findings warrant further in vivo studies to evaluate the potential of this conjugate as photosensitizer for photodynamic therapy (PDT) of cancers overexpressing the GRP receptor.



INTRODUCTION

Multifunctional agents for simultaneous imaging and targeted therapy of cancer, known as theranostics, have become of increasing interest over the past decade. Various noninvasive imaging techniques can be used in tandem with therapeutic modalities for image-guided therapy, and particularly the combination of photodynamic therapy (PDT) and fluorescence imaging has gained growing attention over the last decades.^{1,2} PDT combines a photosensitizer (PS) and light of an appropriate wavelength to impart cytotoxicity via the generation of reactive molecular species.³ The light-induced electronic excitation of a PS can result not only in a cytotoxic effect but also in the emission of fluorescence due to relaxation of the excited-singlet-state PS back to the ground state.⁴ The phenomenon that the same entity (PS) can act both as therapeutic and imaging agent due to ability of the PS to fluoresce is a unique advantage of PDT. The PS's fluorescence can be used in diagnostics, therapy guidance, monitoring, treatment assessment, and mechanistic studies.¹

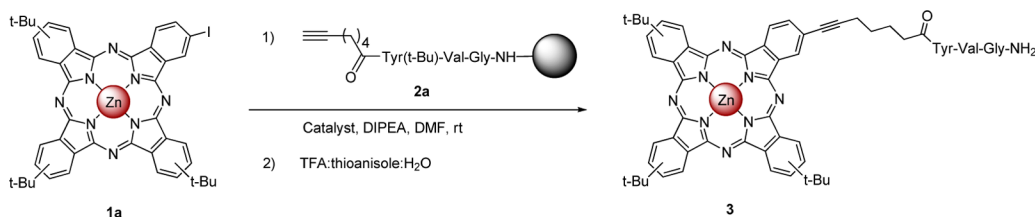
Phthalocyanines (*Pc*) are of particular interest as PS for PDT due to their suitable physical and chemical properties. They can be synthesized in a straightforward manner and modified to alter hydrophilicity, absorption, and emission wavelengths for different applications.^{5,6} *Pc* exhibit high photo- and chemical stability, which is desirable for chemical modifications as well as in vitro and in vivo applications. They show long-wavelength absorption with high extinction coefficients ($\epsilon > 10^5 \text{ M}^{-1} \text{ cm}^{-1}$), red fluorescence emission approaching NIR wavelengths for deeper tissue imaging, and high singlet oxygen quantum yields.⁷ Recent evidence that Raman imaging of *Pc* distribution

can identify malignant areas of a tumor may further contribute to improve *Pc*-PDT effectiveness.⁸ Sulfonated *Pc* (*PcS*) are anionic water-soluble phthalocyanines that are effective PS to kill tumor cells in vitro⁹ and cause tumor regression in vivo.¹⁰ Because of the presence of the negatively charged sulfonate groups, *PcS* show higher water-solubility and reduced aggregation as compared to nonsubstituted *Pc*. Combined these properties make *PcS* attractive PS for PDT as well as molecular probes for fluorescence imaging.

The successful outcome of PDT depends to a large extent on the tissue and intracellular localization of the PS. Nonspecific localization often leads to suboptimal treatment outcome and toxicity to healthy tissues. Therefore, the development of PS with improved specificity, selectivity, and efficacy is highly desirable for the successful PDT of tumors while preserving healthy adjacent tissues. To achieve efficient and reliable delivery of chemotherapeutics and diagnostics to cancer cells, a number of delivery agents have been investigated in recent years.¹¹ Among them, tumor cell-targeting peptides have emerged as the most valuable nonimmunogenic tools. In contrast to larger molecules such as monoclonal antibodies (mAbs), short synthetic peptides have excellent tumor penetration properties, which in combination with their selective binding and rapid internalization, make them ideal carriers of therapeutics to both primary and metastatic tumor sites. Unlike viral delivery vectors and mAbs, peptides are nearly invisible to the immune system and are expected to

Received: September 11, 2012

Published: January 28, 2013

Scheme 1. Solid-Phase Synthesis of ZnPc(*t*-Bu)₃–YVG Conjugate 3

cause minimal or no side effects.¹² Although natural peptides have a short biological half-life, structural modifications of the amino acid sequence can be easily done in order to improve their *in vivo* stability.¹³

Bombesin (BBN) is a 14-amino acid peptide (Tyr-Gln-Arg-Leu-Gly-Asn-Gln-Trp-Ala-Val-Gly-His-Leu-Met-NH₂) showing high affinity for the gastrin-releasing peptide receptors (GRPR). A variety of tumors overexpress receptors to BBN and gastrin, including those of breast, prostate, gastric, colon, pancreatic, and small cell lung cancer.¹⁴ In the case of prostate cancer, the receptor subtype GRPR is expressed early in tumor development and correlated with tumor aggressiveness.¹⁵ BBN analogues have been labeled with both fluorescent moieties, and radioisotopes and *in vitro* and *in vivo* studies confirm their potential for fluorescence imaging, conventional nuclear medicine, or PET imaging as well as radiation-mediated therapy.¹⁶ These analogues generally show good stability, high receptor binding affinity, and rapid tumor uptake.^{17,18} Hence we selected [D-Tyr⁶,βAla¹¹,Thi¹³,Nle¹⁴]bombesin[6–14]NH₂, a potent modified GRPR agonist peptide¹⁹ previously developed by Robert T. Jensen and co-workers as a site-specific delivery agent for *Pc*. We also included the integrin-binding motif arginine–glycine–aspartic acid (RGD) as another interesting peptide carrier for *Pc*. Integrins are a large class of heterodimeric cell surface receptors that are overexpressed on tumor vasculature. RGD is a recognition motif of numerous ligands (fibronectin, collagen, prothrombin, adenovirus penton base protein, vitronectin, as well as many other glycoproteins) for different integrins including α₃β₁, α₅β₁, α₈β₁, α_vβ₁, α_vβ₃, α_vβ₅, α_vβ₆, and α_{11b}β₃.^{20–22} Of these RGD binding integrins, α_vβ₃ and α_vβ₅ have received increasing interest as therapeutic and diagnostic targets^{23,24} because of their role in tumor growth and angiogenesis.²⁵ As a nonspecific peptide that does not target any peptide receptor involved in cancer, we used the tyrosine–valine–glycine (YVG) motif.

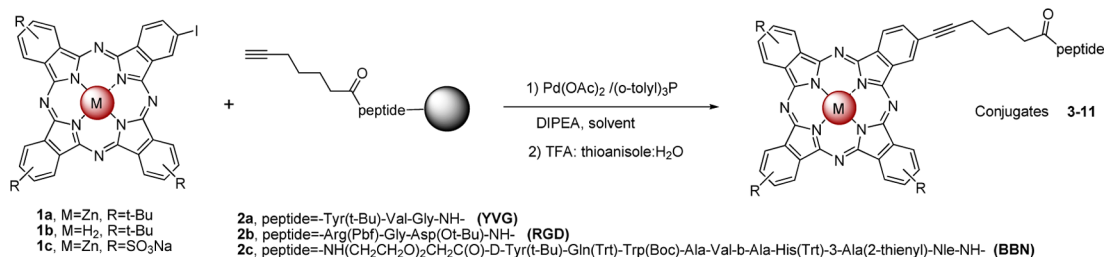
As a carrier for *Pc*, a BBN or RGD peptide moiety can be expected not only to improve cell targeting but also to increase water solubility and reduce aggregation, consequently leading to improved photosensitizing activity and augmented fluorescence. Only a few examples of *Pc* functionalization with peptides have been reported,^{26,27} generally involving peptide bond formation, an approach that is also commonly used for the preparation of covalently linked *Pc*–protein conjugates.²⁸ More recently the conjugation of *Pc* azide linked to solid support and alkyne functionalized peptide was achieved using Click chemistry.²⁹ We recently demonstrated a new strategy for the introduction of *Pc* at the N/C-terminal positions or on a phenylalanine side chain of protected model peptides utilizing palladium-catalyzed cross-coupling reactions.³⁰ Sonogashira cross-coupling is one of the most important and widely used sp²–sp carbon–carbon bond forming reaction in organic synthesis, frequently employed in the synthesis of natural products and biologically active molecules.³¹ We previously

shown that the presence of a carbon–carbon triple bond in the *Pc*S side chain does not affect *in vitro* stability.¹⁰ Very mild conditions and tolerance to different functional groups are among the advantages of this procedure. Hence Sonogashira coupling was a logical target for the development of solid-phase organic synthesis (SPOS) offering several advantages including facile purification by simple filtration.³² Herein we report two alternative strategies to synthesize *Pc*–peptide conjugates based on Sonogashira cross-coupling. First, acetylenic peptides of different lengths and structures (YVG, RGD, BBN[6–14]) linked to a solid support were screened in a solid-phase Sonogashira cross-coupling with different types of iodinated phthalocyanines (metalated or metal-free *Pc*, neutral or anionic *Pc*). Second, the Sonogashira cross-coupling of an iodinated *Pc* with an unprotected acetylenic peptide in solution was investigated. The water-soluble conjugates were then screened for their PDT efficacy against several cancer cell lines expressing different levels of GRPR and integrin receptors, and their intracellular localization was evaluated via confocal fluorescence microscopy. The involvement of receptor-mediated processes in both the PDT action and localization of the PS was verified by receptor blocking experiments.

RESULTS AND DISCUSSION

Solid-Phase Synthesis. Although Sonogashira coupling using aryl-halide or triflate attached to solid support has been extensively applied to SPOS, the alternative method using resin-supported alkyne is less common.²⁴ The first approach we envisaged for the synthesis of *Pc*–peptide conjugates involved Sonogashira coupling of a resin-bound peptide functionalized with the terminal triple bond and an iodinated phthalocyanine. Use of Sonogashira coupling for modification of peptides, while still attached to solid support, seems to be not well-exploited. The “on resin” Sonogashira coupling reaction employed for the macrocyclization of a resin-bound peptide to form a 65-membered ring appears to be the only example found in the literature.³³ In our studies, a hydrophilic, polyethylene glycol-based TGR resin was chosen as a solid support. The application of this type of resin in solid-phase variant of Sonogashira has been previously reported and shown to be advantageous over Rink amide resin (cross-linked polystyrene resin with Rink linker) in some cases.³⁴ Accordingly, the solid-supported acetylenic peptides 2a–2c were synthesized via the Fmoc (fluorenylmethyloxycarbonyl) strategy to be employed in Sonogashira coupling with iodinated *Pc*.

Typical literature procedures for Sonogashira couplings utilize palladium catalyst with a metal cocatalyst and a base. The most widely employed cocatalysts are copper salts which also mediate Hay/Glaser reaction.³⁵ Thus homocoupling of the alkyne is a major problem when the supply of acetylene is limited. Indeed, when our first experiments were carried out using 1a and a resin-supported peptide 2a as a model system under the conditions reported for the cyclization of the resin-

Table 1. Analytical Data for the *Pc*-Peptide Conjugates Obtained via the Solid-Phase Sonogashira Cross-Coupling^a

entry	<i>Pc</i> ^b	peptide	ratio <i>Pc</i> :peptide	product	solvent	[M + H] ⁺		UV-vis λ _{max} nm (DMF)	conversion ^g , %	yield %
						calcd ^d	found ^d			
1	1a	2a	1:2	3	DMF	1189.8 1211.8 ^e	1190.0 1212.6 ^e	348, 612 (sh), 678	80	35
2	1a	2b	1:2	4	DMF	1198.7	1198.5	351, 613 (sh), 679	60 (75 ^c)	21 (30 ^c)
3	1a	2c	1:2	5	THF	2137.9 2159.9 ^e	2138.1 2160.8 ^e	349, 612 (sh), 680	50	10
	1b	2a	1:2	6	THF	1126.4 1148.4 ^e	1126.2 1148.8 ^e	340, 607 (sh), 641 (sh), 665, 698 ^f	75	30
5	1b	2b	1:1.7	7	THF	1135.3	1135.1	344, 610 (sh), 639 (sh), 669, 696	70	30
6	1b	2c	1:1.7	8	THF	2074.5 2096.5 ^e	2074.7 2097.0 ^e	344, 610 (sh), 638 (sh), 670, 694	30	10
7	1c	2a	1:3	9	DMF ^c	1261.6 1283.6 ^e	1261.7 1283.7 ^e	354, 613 (sh), 680	50	11
8	1c	2b	1:3	10	DMF ^c	1270.6	1270.9	352, 614 (sh), 681	54	16
9	1c	2c	1:3	11	DMF ^c	2209.7	2209.9	355, 614 (sh), 681	20	2

^aConditions: TGR resin (1.5–3 equiv), *Pc* (1 equiv), Pd(OAc)₂ (50 mol %), (*o*-tolyl)₃P (150 mol %), DIPEA (15 equiv), rt, 2 d. ^bIt should be noted that the *Pc* **1a**–**1c** were obtained via statistical condensation and consequently are composed of mixtures of positional isomers. ^cThe reaction was run for 1 d at 80 °C. ^dAverage mass values obtained by MALDI-TOF spectroscopy. ^eMass value is given for [M + H]⁺ adduct. ^fTHF was used as a solvent. ^gThe conversion of *Pc* to *Pc*-peptide conjugate was estimated from the amount of *Pc* left in the solution and calculated based on the molar amount of starting *Pc*.

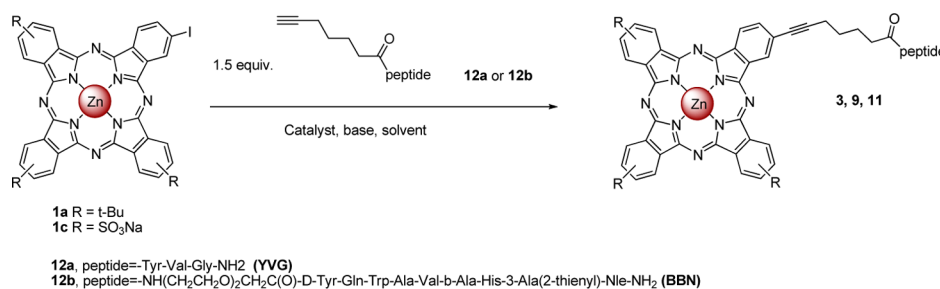
bound peptide via solid-phase Sonogashira coupling [Pd-(PPh₃)₂Cl₂ (10 mol %), PPh₃ (20 mol %), CuI (20 mol %)],²⁹ the desired product **3** was formed in moderate ~25% yield along with the product of Glazer coupling as a major compound (Scheme 1).

This result was somewhat surprising as less favorable interference between alkynes linked to the solid support was expected. Thus it is well-known that under the conditions of solid-phase Sonogashira coupling, the oxidative dimerization of alkyne is almost avoided when the acetylenic reactant is covalently bound to the polymer.³⁶ To confirm our result, a test experiment was performed: the reaction was repeated using the same conditions but omitting the addition of *Pc*. After one day at room temperature, only a few percent of starting peptide remained whereas the diyne appeared as a major compound. Considering these results, copper-free Sonogashira coupling conditions³⁷ were then tried. Reacting 1.5 equiv of **1a** with the on-bead **2a** in the presence of Pd(OAc)₂, a bulky, electron-rich tri(*o*-tolyl)phosphine [(*o*-tolyl)₃P] and *N,N*-diisopropylethylamine [DIPEA] in *N,N*-dimethylformamide (DMF) resulted in the formation of the desired product in 60% crude yield, meaning that only 40% of *Pc* was converted into the conjugate **3**. We subsequently inverted the *Pc*:peptide ratio and performed the reaction of **1a** with 2 equiv of solid-supported **2a**, resulting in 80% conversion of *Pc* into conjugate **3**. We also performed the same reaction in 5% v/v aqueous/DMF solution to test the sensitivity of the reaction to water. This resulted in a decrease of *Pc* conversion to desired conjugate, confirming that

the reaction is indeed sensitive to water. For the best result, the reaction should be performed under anhydrous conditions and inert atmosphere, with special attention being paid to careful degassing all the solvents and reagents. The quality of solvent used in the reaction has been observed to play an important role as well; in all the reactions described herein, anhydrous amine-free solvent was employed. It should also be noted that in all the reactions the recuperated phthalocyanine was the reduction product and not the starting iodinated phthalocyanine.

To examine the general applicability of our approach, we performed a series of experiments employing different peptides and phthalocyanines (Table 1). The coupling of neutral **1a** and **1b** with solid-supported peptides was carried out at room temperature for two days, while all the reactions of **1c** with peptides were performed at 80 °C for one day. Generally, peptide was taken in excess to achieve higher conversion of *Pc* to an appropriate conjugate.

tert-Butyl-substituted ZnPc **1a** was successfully coupled with the on-bead model YVG-peptide **2a** and the RGD-peptide **2b** to give the corresponding conjugates **3** and **4** in moderate 30–35% yields (Table 1, entries 1, 2). The coupling in DMF of the solid-supported BBN **2c** and **1a** gave only trace amount of the desired product, whereas the reaction in THF resulted in 50% conversion of **1a** to the *Pc*-BBN conjugate **5**, which was isolated in 10% yield (Table 1, entry 3). Similarly, the cross-coupling of metal-free **1b** with the resin-bound tripeptides **2a** and **2b** gave the corresponding conjugates **6** and **7** in moderate

Table 2. Synthesis of Water-Soluble *Pc*-Peptide Conjugates 9, 11, and Organo-soluble Conjugate 3 via the Sonogashira Cross-Coupling in Solution^a

entry	<i>Pc</i>	peptide	product	catalyst	base	solvent	<i>T</i> [°C]	time [h]	conversion ^b [%]	yield [%]
1	1c	12a	9	5 mol % Pd(OAc) ₂ /25 mol % TPPTS		50 mM NaOAc buffer, pH 5.5	rt	24	traces	
2	1c	12a	9	10 mol % Pd(OAc) ₂ , 30 mol % TXPTS, 10 mol % CuI	Et ₃ N	1:1 H ₂ O: CH ₃ CN	80	1	85	
3	1c	12a	9	50 mol % Pd(OAc) ₂ , 150 mol % (<i>o</i> -tolyl) ₃ P	EtN(<i>i</i> -Pr) ₂	DMF	70	1	90	70
4	1c	12b	11	50 mol % Pd(OAc) ₂ , 150 mol % TXPTS, 5 mol % CuI	Et ₃ N	1:1 H ₂ O: CH ₃ CN	80	24	traces	
5	1c	12b	11	50 mol % Pd(OAc) ₂ , 150 mol % TXPTS, 5 mol % CuI	EtN(<i>i</i> -Pr) ₂	1:1 H ₂ O: DMF	80	12	65	
6	1c	12b	11	50 mol % Pd(OAc) ₂ , 150 mol % (<i>o</i> -tolyl) ₃ P	EtN(<i>i</i> -Pr) ₂	DMF	70	1	75	50
7	1a	12a	3	50 mol % Pd(OAc) ₂ , 150 mol % (<i>o</i> -tolyl) ₃ P	EtN(<i>i</i> -Pr) ₂	DMF ^b	70	1	quant ^c	60

^aReactions were run under conditions given in the table. ^bConversion of *Pc* to the cross-coupled product was estimated from HPLC profile of the reaction mixture, unless otherwise stated. ^cConversion was estimated by TLC (SiO₂, CH₂Cl₂:MeOH 10:1).

30% yields (Table 1, entries 4, 5), while the *Pc*-BBN conjugate **8** was isolated in 10% yield (Table 1, entry 9). The reactions of the metal-free **1b** with the peptides **2a** and **2b** were carried out in tetrahydrofuran (THF) because of the low solubility of **1b** in DMF. However, when the anionic **1c** was subjected to copper-free Sonogashira coupling with the solid-supported **2a** in DMF at room temperature for two days, only trace amounts of the desired conjugate **9** were formed, together with the homocoupling product. But, when the reaction was heated at 80 °C for one day, the desired product **9** was isolated in 11% yield (Table 1, entry 10). Similarly, the reaction of **1c** with the on-resin RGD-peptide **2b** at elevated temperature gave the target conjugate **10** in 16% (Table 1, entry 11). However, when trying to couple the on-bead bombesin **2c** with **1c** under optimized conditions, the desired conjugate **11** was isolated in only 2% yield (Table 1, entry 12). We speculate that the rather low isolated yields of the coupling products **9–11** considering the quite high estimated conversion of *Pc* to the conjugates might be caused by instability of the TentaGel support at elevated temperatures. Indeed, Hutchins and Chapman, when describing Fisher indole synthesis on a solid support, reported that at higher temperatures the yields began to decline and impurities related to the PEG grafted solid support became problematic.³⁸

Although the yields of the *Pc*-peptide conjugates obtained via solid-phase synthesis are relatively moderate, the method offers an advantage of rather ease of product purification. After the reaction is completed, the reduced product, catalyst, and base are removed by simple filtration followed by a cleavage of reaction products from the resin with the TFA:H₂O:thioanisole (92:2:6, v/v/v) cocktail. The purification of the *Pc*-peptide

conjugates from starting peptides and/or peptide homodimers can be performed rather easily via two-step reversed-phase high-performance liquid chromatography (RP-HPLC). At first, peptides are eluted with a 0–100% linear gradient of CH₃CN in water (containing 0.05% TFA) in 20 min while *Pc*-peptide conjugates remain on the column. Afterward, *tert*-butyl substituted *Pc*-peptide conjugates are eluted with THF whereas sulfonated derivatives are eluted with a linear gradient of 0–100% MeOH in phosphate buffer (10 mM, pH 5) in 40 min.³⁹

Generally, the yields of the *Pc*-peptides conjugated with shorter peptides such as YVG and RGD are higher (30–35% for *tert*-butyl substituted *Pcs*, 11–16% for sulfonated *Pc*) than those with longer peptide BBN (6–14) (10% for *tert*-butyl substituted *PcS*, 2% for sulfonated *Pc*). The coupling of sulfonated *Pc* **1c** with on-bead peptides is not favored at room temperature and requires elevated temperatures. However, the instability of the solid support at elevated temperatures gives rise to rather low isolated yields of the desired products. The yields can be likely improved by substitution of TGR resin for another solid support with higher thermal stability.

Synthesis in Solution. An alternative strategy that we explored for the synthesis of *Pc*-peptide conjugates was based on Sonogashira coupling of unprotected acetylenic peptide and iodinated *Pc* in solution. It has been previously demonstrated that Sonogashira cross-coupling on proteins allows the regioselective linking of iodo-aryl and alkyne moieties because these groups are orthogonal in their reactivity to almost all other functional groups in proteins.⁴⁰ Bong and Ghadiri⁴¹ reported the efficient chemoselective Pd(0)-catalyzed Sonogashira coupling of synthetic peptides of 17- and 33-residue

length bearing iodo-phenyl moieties to a trialkyne in water employing catalyst derived from Pd(OAc)₂ and commercially available trisodium tri(3-sulfonatophenyl)phosphane (TPPTS). The authors showed that peptides containing free amines, carboxylates, guanidines, hydroxyls, and thioesters were efficiently coupled to a trialkyne, whereas the presence of free thiols, thioethers, and bipyridyl moieties was not tolerated. In our preliminary experiments, model peptide **12a** was allowed to react with water-soluble trisulfonated *Pc* **1c** in 1:1.1 ratio under the reported conditions (Table 2, entry 1). In contrast to our expectations, only traces of the desired conjugate **9** were detected using MALDI-TOF spectroscopy even after prolonging the reaction for one day, while the bulk of the starting peptide remained unreacted. More recently, Cho and co-workers reported markedly higher activity of the catalyst derived from more bulky trisodium tri(2,4-dimethyl-5-sulfonatophenyl)phosphane (TXPTS) compared to catalyst formed from TPPTS in the Sonogashira coupling of nucleosides.⁴² They found that the reaction was the most efficient when stirring alkyne and halonucleoside in 2:1 ratio in the presence of 10 mol % Pd(OAc)₂, 10 mol % CuI, 30 mol % TXPTS, and 1 equiv of triethylamine in 1:1 H₂O:CH₃CN at 80 °C for 1 h. The same authors noted that at least one equivalent of base was required for the reaction albeit higher concentrations of base did not affect the catalyst performance. We employed the reported conditions (Table 2, entry 2) for the coupling of **12a** with **1c** in 1.5:1 ratio. The reaction was complete within 1 h, and the formation of the cross-coupled product **9** was confirmed by MALDI-TOF spectroscopy and analysis of RP-HPLC profile of the reaction mixture at 223 and 675 nm. When we employed the copper-free Sonogashira coupling conditions for the same reaction, a similar reaction course was observed. Compound **1c** was allowed to react with the peptide **12a** in DMF at 70 °C in the presence of Pd(OAc)₂, (*o*-tolyl)₃P, and DIPEA (Table 2, entry 3). Monitoring the reaction showed the clean formation of the cross-coupled product **3** in 90% yield within 1 h (Supporting Information Figure S41). However, when acetylenic bombesin **12b** was subjected to a reaction with water-soluble **1c** in the presence of 10 mol % Pd(OAc)₂, 10 mol % CuI, 30 mol % TXPTS, and 5 equiv of triethylamine in 1:1 H₂O:CH₃CN, almost no **1c** consumption was observed even after 24 h of stirring. Increasing the catalyst loading (50 mol % Pd(OAc)₂ and 150 mol % TXPTS) gave only traces of the desired conjugate **11** along with starting *Pc*, while a peak of the starting peptide completely disappeared in the HPLC trace of the reaction mixture (Table 2, entry 4). This failure can probably be attributed to some heterogeneity of the reaction; BBN **12b** is not sufficiently soluble in the reaction mixture. Using DMF instead of acetonitrile drastically changed the course of the reaction; the desired product was formed in ~65% in the reaction mixture when **12b** was allowed to react with **1c** in 1:1 H₂O:DMF in the presence of 50 mol % Pd(OAc)₂, 5 mol % CuI, 150 mol % TXPTS, and 5 equiv of triethylamine, at 80 °C overnight (Table 2, entry 5). The copper-free Sonogashira conditions afforded the desired conjugate **11** in ~75% crude yield along with the reduced product after the reaction was stirred at 70 °C for 1 h (Table 2, entry 6, Supporting Information Figure S48). Similarly, the organo-soluble conjugate **3** was easily prepared from **1a** and **12a** in good yield using the optimized copper-free conditions (Table 2, entry 7). The purification of water-soluble conjugates **9** and **11** was achieved via two-step RP-HPLC: at first the unreacted

peptide and/or peptide homodimer was eluted with a 0–100% linear gradient of CH₃CN in water (containing 0.05% TFA) in 20 min while *Pc*-peptide conjugates remained on the column. Then a linear gradient of 0–100% MeOH in phosphate buffer (10 mM, pH 5.0) in 40 min was employed in order to purify the target compound from the reduction product and catalyst. Following this procedure, the desired conjugates **9** and **11** were isolated in ~70 and ~50% yields, respectively. The organo-soluble conjugate **3** was purified by flash chromatography on silica using 1–10% gradient of MeOH in CH₂Cl₂. In summary, we have demonstrated that both Sonogashira coupling on solid phase and in solution are feasible routes to *Pc*-peptide conjugates.

Cell Lines. Cell lines used in these studies express different levels of the GRPR and integrin receptors, including the estrogen-independent human breast cancer cell line MDA-MB-231, human lung adenocarcinoma A549, androgen-independent human prostate cancer PC-3, and murine mammary carcinoma EMT-6. The expression of the integrin α_v by MDA-MB-231, PC-3, and A549 cells is well documented using various standard methods^{43–45} but has not been reported for EMT-6 cells. With regard to the expression of subtype integrins $\alpha_v\beta_1$, $\alpha_v\beta_3$, $\alpha_v\beta_6$, and $\alpha_v\beta_5$ by MDA-MB-231 cells, reports are controversial. Thus in some publications, MDA-MB-231 expresses high integrin $\alpha_v\beta_3$ receptor levels and undetectable amounts of GRPR.⁴⁶ Other studies support the expression of $\alpha_v\beta_5$ and $\alpha_v\beta_1$ but detect no significant levels of $\alpha_v\beta_3$ and $\alpha_v\beta_6$.⁴⁴ GRPR levels in MDA-MB-231 are detected in moderate levels, comparable to those found in PC3 cells.⁴⁷ A549 cells express very low levels of GRPR⁴⁸ but high levels of integrin α_v , in particular $\alpha_v\beta_1$, $\alpha_v\beta_3$ receptors that exert a high binding affinity for the RGD motif.⁴³ The PC-3 prostate cancer cell line has been used extensively as in vitro and in vivo models to evaluate the receptor-mediated uptake of fluorescent or radiolabeled BBN conjugates.⁴⁹ This cell line expresses high levels of GRPR that are 1000× higher than those of the integrin $\alpha_v\beta_3$ receptor density (e.g., 2.70×10^6 vs 2.76×10^3 receptors/cell).⁵⁰ Literature values for surface expression of α_2 , α_3 , α_6 , β_1 , and β_4 integrin subunits, and mRNA expression of α_6 , β_1 , and β_4 by PC-3 cells, were established by flow cytometry and Northern blot analysis, respectively.⁵¹ Finally, EMT-6 murine mammary carcinoma cells were selected as a control because they express very little integrin $\alpha_v\beta_3$.^{52–54}

To verify the content of α_3 , $\alpha_v\beta_3$, $\alpha_v\beta_5$, and GRPR by the selected cell lines, we investigated their expression by Western blot (Supporting Information Figure S45). Their concentrations were calculated relative to the β -actin concentration using Image J software (Table 3). Our results show that all the four cell lines express high levels of integrin α_3 . The integrin/ β -

Table 3. Receptor Concentration Relative to β -Actin as Determined by Western Blot

receptors ^a	cell lines			
	PC3	EMT-6	A549	MDA-MB-231
GRPR glycosylated	2.88	0.92	1.42	0.29
GRPR endogenous	1.78	1.04	1.53	1.35
α_3	1.57	0.61	2.82	1.63
α_v	0.79	0.10	0.91	1.05
β_3	0.15	0.10	0.13	0.92
β_5	0.60	0.09	1.60	1.08

^aGRPR or integrin concentrations relative to β -actin as determined by Image J software analysis.

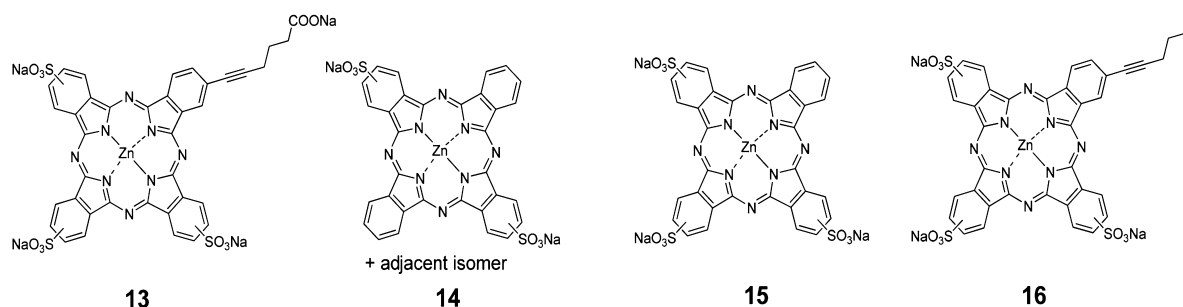


Figure 1. Structures of the reference phthalocyanines.

Table 4. Cell Uptake and Phototoxicity of ZnPc Derivatives

cell lines ^a	ZnPc	LD ₅₀ ^b (J cm ⁻²)	cell uptake ^c (nmol Pc/mg protein)	cells killed per photon absorbed ^d (%)
PC3	ZnPcS ₃ C ₅ -COOH (13)	9.31 ± 0.60	0.38 ± 0.06	8.47
	ZnPc-BBN (11)	1.81 ± 0.20	0.78 ± 0.12	98.25
	ZnPc-RGD (10)	16.16 ± 0.74	0.26 ± 0.04	4.58
	ZnPc-YVG (9)	9.83 ± 0.76	1.93 ± 0.29	0.00
	ZnPcS ₂ (14)	0.52 ± 0.03	4.76 ± 0.71	66.44
	ZnPcS ₃ C ₆ (16)	2.20 ± 0.28	2.82 ± 0.36	59.08
	ZnPcS ₃ (15)	9.19 ± 0.64	0.35 ± 0.05	8.25
A549	ZnPcS ₃ C ₅ -COOH (13)	15.49 ± 1.84	0.66 ± 0.10	3.3
	ZnPc-BBN (11)	3.70 ± 0.46	0.61 ± 0.09	1.9
	ZnPc-RGD (10)	26.45 ± 2.44	0.47 ± 0.07	0.0
	ZnPc-YVG (9)	7.76 ± 0.38	0.70 ± 0.11	0.0
	ZnPcS ₂ (14)	0.52 ± 0.03	1.84 ± 0.27	91.3
	ZnPcS ₃ C ₆ (16)	2.30 ± 0.24	2.53 ± 0.38	37.7
	ZnPcS ₃ (15)	8.71 ± 0.77	0.69 ± 0.10	1.6
MDA-MB-231	ZnPcS ₃ C ₅ -COOH (13)	7.95 ± 0.37	0.33 ± 0.05	21.22
	ZnPc-BBN (11)	2.78 ± 0.17	0.53 ± 0.08	36.86
	ZnPc-RGD (10)	10.21 ± 1.00	0.41 ± 0.06	22.17
	ZnPc-YVG (9)	9.59 ± 0.94	0.01 ± 0.00	0.00
	ZnPcS ₂ (14)	0.24 ± 0.08	0.53 ± 0.08	50.81
	ZnPcS ₃ C ₆ (16)	0.91 ± 0.06	0.20 ± 0.03	50.46
	ZnPcS ₃ (15)	5.52 ± 0.42	1.00 ± 0.15	28.87
EMT-6	ZnPcS ₃ C ₅ -COOH (13)	8.43 ± 0.69	0.73 ± 0.11	0.00
	ZnPc-BBN (11)	4.48 ± 0.51	0.91 ± 0.14	7.40
	ZnPc-RGD (10)	16.13 ± 1.97	0.59 ± 0.09	0.00
	ZnPc-YVG (9)	5.33 ± 0.60	1.11 ± 0.17	0.00
	ZnPcS ₂ (14)	0.69 ± 0.08	3.72 ± 0.56	93.41
	ZnPcS ₃ C ₆ (16)	2.24 ± 0.27	1.02 ± 0.15	25.44
	ZnPcS ₃ (15)	8.62 ± 0.47	1.58 ± 0.24	37.17

^aThe relative concentrations of GRPR and integrin receptors are summarized in Table 4. ^bTumor cells were incubated with the various ZnPc derivatives (2 μM) for 24 h prior to PDT. LD₅₀ values represent the fluence required for 50% cell survival, calculated from the survival curves presented in Supporting Information (Figure S52). ^cTumor cells were incubated with the various ZnPc derivatives (2 μM) for 24 h prior to extraction. ^dThe % of cells killed/photon absorbed were calculated from cell survival after exposure to 3 J·cm⁻² and by taking into account cell uptake and absorbance of the different conjugates.⁵⁵

actin ratios derived from the Western blots indicate that the relative level of integrin expression respects the following order: MDA-MB-431 ≈ A549 > PC-3 > EMT-6 (Table 3). The expression of α_v was detected in all cell lines, although in very low levels in EMT-6. Integrin α_vβ₃ levels were detected only in MDA-MB-231 cells. None of the other three cell lines tested expressed substantial levels of this receptor, including the A549 line, which confirms reported data.⁴³ In contrast, α_vβ₅ expression was shown to be substantially higher in A549 cells as compared to levels found in MDA-MB-231 cells, while low

levels were detected in PC-3 cells and none in EMT-6 cells. GRPR endogenous was expressed by all four cell lines (PC-3 ≥ A549 > MDA-MB-231 ≫ EMT-6), but the GRPR glycosylated form was absent in MDA-MB-231 cells while present in the other three cell lines (PC-3 ≫ A549 > EMT-6).

Photocytotoxicity and Cellular Uptake. The cellular uptake results for the water-soluble ZnPc-peptide conjugates 9–11, as well as the reference phthalocyanines, e.g., the carboxylated analogue ZnPcS₃C₅COOH (13), disulfonated ZnPcS₂ (14), trisulfonated ZnPcS₃ (15), and ZnPcS₃C₆ (16)

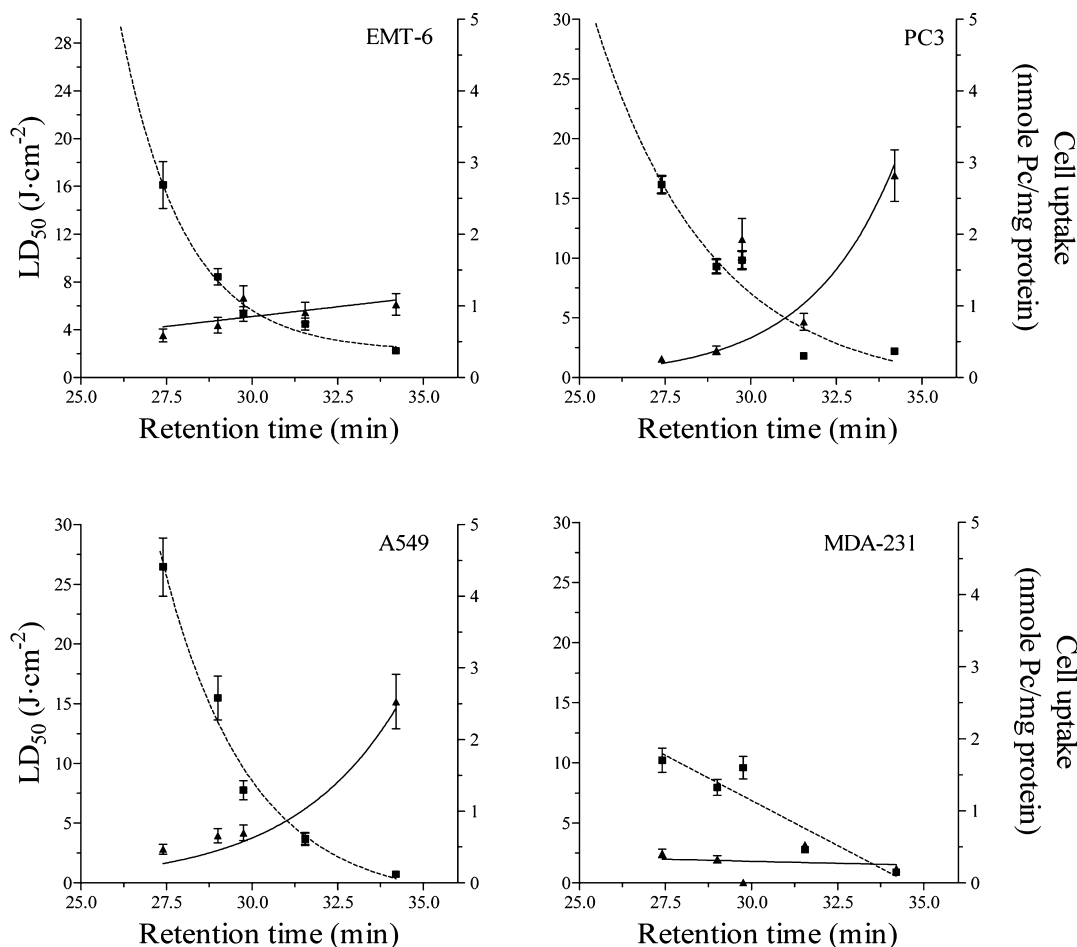


Figure 2. Comparison of LD_{50} (■) and cell uptake of *Pc*-peptide conjugates after 24 h incubation (▲) with different cell lines vs retention times on a C18 reversed-phase HPLC column. Retention times and *n*-octanol/water partition coefficients of substituted *PcS* show a linear correlation¹⁰ and can be used as a measure of the relative hydrophobicity of the *PcS* and their peptide conjugates. Retention times of the conjugates and reference *Pc* are: 27.4 min, Zn*Pc*-RGD (10); 29.0 min, Zn*PcS*₃C₅-COOH (13); 29.8 min, Zn*Pc*-YVG (9); 31.6 min, Zn*Pc*-BBN (11) and 34.2 min, Zn*PcS*₃C₆ (16).

(Figure 1) by four different tumor cell lines after 24 h incubation with 2 μ M PS, together with the light dose required for 50% cell survival (LD_{50}), are summarized in Table 4.

The average LD_{50} s, together with the standard deviation, were estimated with Prism graph software from the survival curves presented as Supporting Information (Figure S52). The phototoxicity is also expressed as number of cells killed per photon absorbed (Table 4) by calculating cell survival after exposure to 3 $J \cdot cm^{-2}$ and by taking into account cell uptake and absorbance of the different conjugates. To illustrate a possible correlation between the hydrophobicity of the *Pc*-peptide conjugates and phototoxicity, the LD_{50} and cell uptake values were plotted against the HPLC retention times on a reversed phase column (Figure 2).

We have previously shown that the photocytotoxicity of sulfonated Zn*Pc* depends on cellular uptake and intracellular localization, which in turn correlates to the overall hydrophobicity of the derivatives.^{9,10} Using the retention time (t_R) on a reversed-phase HPLC column as a measure of relative hydrophobicity, the three Zn*Pc*-peptide conjugates 9–11, when compared to the nonconjugated Zn*PcS*₃C₅-COOH (13) and Zn*PcS*₃C₆ (16) analogues, are shown likewise to obey this structure–activity relationship (SAR) in all four cell lines tested (Figure 2). Thus the most hydrophilic RGD conjugate 10 ($t_R =$

27.4 min) is the least phototoxic (e.g., highest LD_{50}) in each cell line, coinciding with the lowest level of cell uptake. Only in the MDA-231 cell line, this correlation is less evident, which is largely due to the relative low uptake of all PS tested in this cell line. The photocytotoxicity decreases with decrease in hydrophobicity as observed for the other cell lines. The highest cellular uptake paired with low LD_{50} is observed with the nonconjugated Zn*PcS*₃C₆ (16) parent compound (Figure 2).

However, when expressing photocytotoxicity at a fixed light dose as the percentage of cells killed per photon absorbed, a new SAR emerges, indicative of the involvement of a receptor binding parameter in the overall PDT response (Table 4). Thus, the amphiphilic, nonconjugated Zn*PcS*₂ (14) and Zn*PcS*₃C₆ (16) as well as the hydrophilic Zn*PcS*₃ (15) show high percentages of cell kill in the receptor-poor EMT-6 cells while all Zn*Pc*-peptide conjugates (9, 10 and 11) as well as Zn*PcS*₃C₅-COOH (13) exhibit strongly reduced activity. In contrast, in both GRPR-rich PC3 and MDA-231 cell lines, the Zn*Pc*-BBN conjugate 11 shows a high percentage cell kill. Likewise, the Zn*Pc*-RGD conjugate 10 shows a high percentage of cell kill in the integrin-rich MDA-231 cell line, while this conjugate is inactive in EMT-6 cells that lack this receptor. The RGD-specific integrin receptor ($\alpha_v\beta_3$) is highly expressed in the MDA-231 cell line, while PC3 and A549 cells

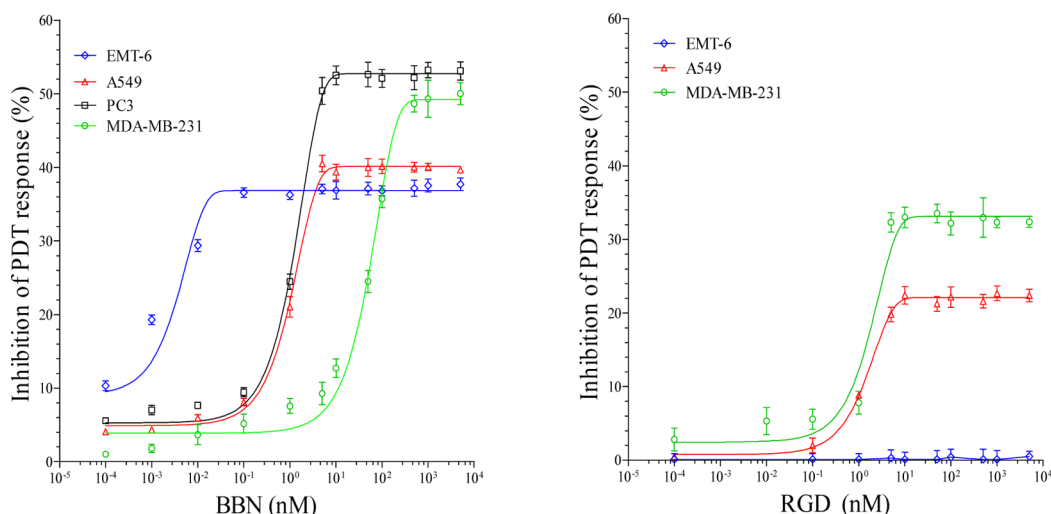


Figure 3. Inhibition of PDT response by BBN and RGD. Left graph: PDT response with ZnPc-BBN (**11**) as PS and BBN as inhibitor. Right graph: PDT response with ZnPc-RGD (**10**) as PS and RGD as inhibitor. Cell lines: in EMT-6 (blue diamonds), A549 (red triangles), PC3 (black squares), and MDA-MB-231 (green circles).

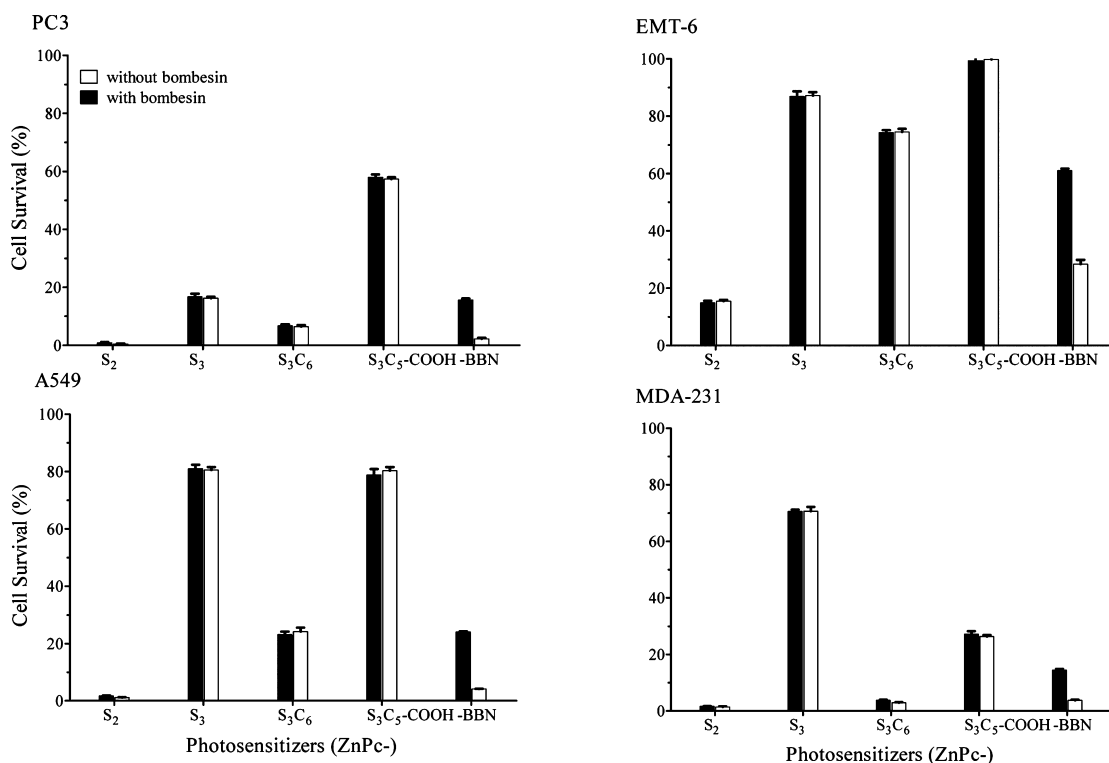


Figure 4. Effect of preincubation with 1 nM BBN on cell survival of EMT-6, A549, PC3, and MDA-MB-231 cells after PDT ($12 \text{ J} \cdot \text{cm}^{-2}$) using ZnPc-BBN (**11**) and several nonconjugated reference *Pc* as photosensitizers: ZnPcS₃C₅COOH (**13**), ZnPcS₂ (**14**), ZnPcS₃ (**15**), and ZnPcS₃C₆ (**16**).

express only $\alpha_v\beta_5$ receptors that exhibit lower affinity for the RGD peptide (Table 3).⁴³ This correlates with the high cell kill observed with the RGD conjugate **10** in MDA-231 cells (Table 4). Furthermore, the highest percentage cell kill (98%) was observed with the BBN conjugate **11** in the case of the PC-3 prostate cancer cell line, while the RGD conjugate **10** showed low activity in this cell line. Conjugation of the ZnPc with YVG (**9**) reduced the PDT efficacy substantially, as indicated by the negligible number of cells killed per photon absorbed for all four cell lines studied (Table 4). These data also confirm the

nonspecificity of compound **9** for either the GRPR or integrin receptors.

Inhibiting PDT Efficacy with BBN or RGD. The involvement of a receptor-mediated photodynamic response using the RGD conjugate **10** and the BBN conjugate **11** on the different cell lines was evaluated by preincubating the cells with either free RGD or BBN prior to the photoinactivation assay. For this assay, a light dose of $12 \text{ J} \cdot \text{cm}^{-2}$ was selected to ensure adequate cell inactivation with all four cell lines. Figure 3 shows the effect of BBN or RGD on the photodynamic activity of ZnPc-BBN (**11**) (left panel) and ZnPc-RGD (**10**) (right

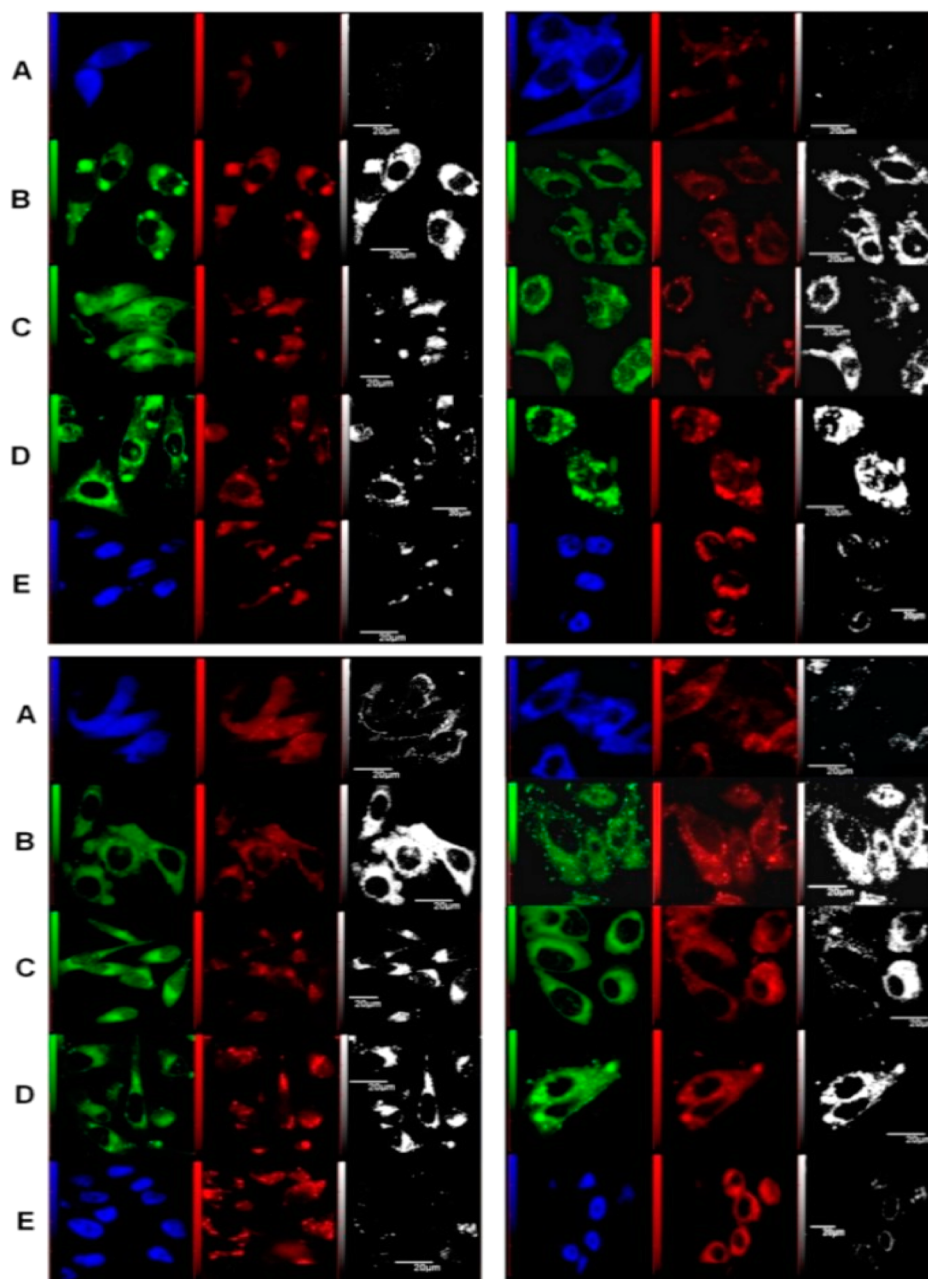


Figure 5. Confocal fluorescence microscopy images of selected MDA-MB-231 (left panels) and PC3 (right panels) cells after 24 h incubation with ZnPc–RGD (**10**) (top panels, red fluorescence) and ZnPc–BBN (**11**) (lower panels, red fluorescence), and various tracker dyes (blue and green fluorescence), including TMADPH for plasmic and endocytic membranes (A), Lyso-Tracker Green for lysosomes (B), Myto-Tracker Green for mitochondria (C), NBDC6 Ceramide for golgi (D), and DAPI for the nucleus (E). Colocalization of ZnPc and tracker dye is presented as white fluorescence.

panel), respectively. The PDT inhibition shows a reversed sigmoid curve indicative of a receptor-blocking, cell type-dependent relationship. The concentration of BBN required to block 50% of the maximum PDT response (IC_{50}) for each cell line increases in the following order: EMT-6 (4.0 ± 0.1 pM) \ll A549 \sim PC3 (1.2 ± 0.2 nM) < MDA-MB-231 (53 ± 5 nM). The order differs slightly from that observed for the GRP receptor content, where MDA-MB-231 express lower GRPR levels as compared to PC3 or A549 cells (Table 3). This confirms that BBN can interact with other receptors expressed by these cell lines and/or that nonspecific cell uptake is involved. In the case of RGD, no effect was observed on the EMT-6 cell line that only expresses negligible levels of $\alpha_v\beta_3$ and

$\alpha_v\beta_5$ receptors (Table 3). In contrast, we observed 50% decrease in PDT response for the RGD receptor positive cell lines A549 and MDA-MB231 (Table 3) at similar RGD concentration (1.56 ± 0.33 and 1.88 ± 0.29 nM, respectively).

In the case of the ZnPc–RGD (**10**), using the receptor-poor EMT-6 cells, no RGD inhibition of PDT response could be observed, even at the maximum concentration of 0.5 μ M used in these experiments (Figure 3, right graph). With the MDA-MB-231 and A549 cell lines that both express the RGD receptor, PDT response could be inhibited up to 34% and 22%, respectively, with IC_{50} RGD concentrations of 1.6 ± 0.7 nM (the IC_{50} is defined as the concentration inhibiting 50% of PDT response). In the case of the bombesin analogue ZnPc–BBN

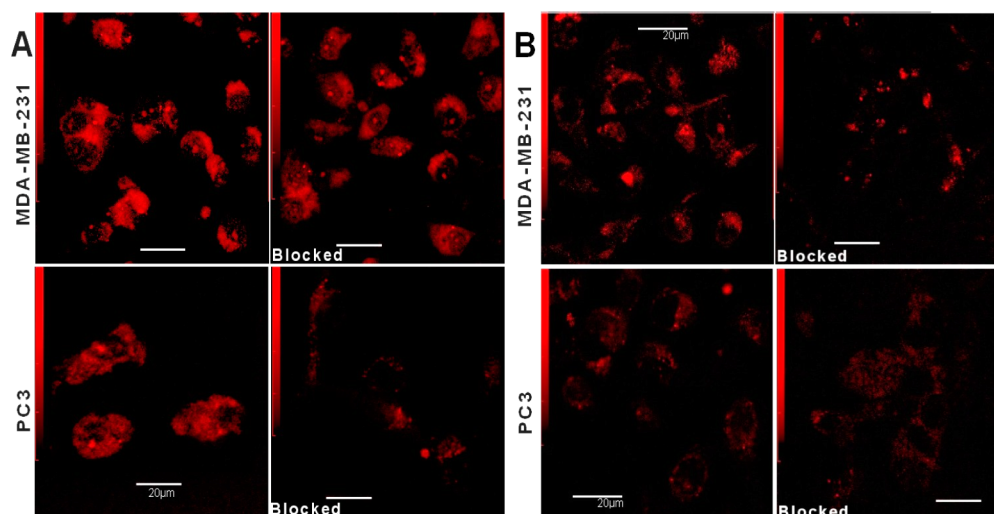


Figure 6. PC3 and MDA-MB-231 cellular uptake visualized by confocal fluorescence microscopy. Effect of preincubation: (A) with 1 nM BBN on ZnPc-BBN (**11**) uptake, (B) with 1 nM RGD on ZnPc-RGD (**10**) uptake.

(**11**), PDT efficacy could be inhibited in all four cell lines by the addition of free BBN, e.g., up to 52% with the GRPR-rich PC3 cells ($IC_{50} = 1.4 \pm 0.1$ nM), 48% with the MDA-MB-231 cells ($IC_{50} = 53 \pm 4.9$ nM), 40% with the A549 cells ($IC_{50} = 1.0 \pm 0.3$ nM), and 35% with the EMT-6 cells ($IC_{50} \sim 4 \pm 0.1$ pM) (Figure 3, left graph). The lower IC_{50} value observed with the EMT-6 cells likely reflects the presence of low concentrations of the GRPR, in accordance with the receptor levels detected by our Western blot analysis (Table 3). EMT-6 cell growth inhibition by vaccine that specifically targets GRPR also suggests the presence of low levels of this receptor.⁵⁶

The role of the BBN receptor in the PDT response obtained with ZnPc-BBN (**11**) was verified on all four cell lines by comparing the latter's activity with that of nonconjugated analogues (Figure 1), e.g., ZnPcS₂ (**14**), ZnPcS₃ (**15**), ZnPcS₃C₆ (**16**), and ZnPcS₃C₅COOH (**13**), with and without addition of 1 nM BBN (Figure 4). Prior incubation with free BBN only affected cell survival after PDT in the case of conjugate **11**, confirming the involvement of a substantial receptor-mediated component in the PDT response induced by this new ZnPc-BBN conjugate. Our data also indicate that all four cell lines express the GRPR to some extent and that the level of BBN inhibition correlates to the level of BBN receptor expression by each cell line (Table 3). These data also exclude a possible involvement of free BBN on nonspecific cell uptake of the nonconjugated ZnPc.

Intracellular Distribution. The intracellular localization of ZnPc-RGD (**10**) and ZnPc-BBN (**11**) was studied in the two receptor-positive PC3 and MDA-MB-231 cell lines (Figure 5). The extent of colocalization with various tracker dyes was estimated by superimposing fluorescence images with those of the following tracker dyes: DAPI for the nucleus, Myto-Tracker Green for mitochondria, Lyso-Tracker Green for lysosomes, NBDC6 Ceramide for Golgi, and TMADPH for membranes. The presence of the ZnPc-peptide conjugates **10** and **11** is evident from their red fluorescence, while tracker dyes are detected by their intense green or blue fluorescence. Colocalization is presented as white coloration as determined with FluoView software. Both the ZnPc-RGD (**10**) and ZnPc-BBN (**11**) conjugates localize at various intracellular organelles and membrane structures in a similar pattern as previously demonstrated for the nonconjugated sulfonated

ZnPcS₃C₆ (**16**).¹⁰ This latter study showed that **16** mainly localized in the cytoplasm, e.g., mitochondria, Golgi, and lysosomes, while almost excluded from the cell nucleus.

Peptide conjugation of ZnPcS₃C₆ (**16**) increases plasmic and perinuclear membrane localization, reflecting cell uptake by integrin and GRP receptor-mediated processes, while localization at the mitochondria, Golgi, and lysosomes reveals that part of the cellular uptake involves passive diffusion and nonspecific endocytosis.

The receptor mediated cellular uptake of the RGD and BBN conjugates **10** and **11** is also evident from blocking experiments (Figure 6). These images show that preincubation of the receptor-rich PC3 and MDA-MB-231 cells (Table 3) with RGD or BBN reduces the red fluorescence from the ZnPc-peptide conjugates. This reduction in intracellular localization is particularly strong in the case of BBN with the ZnPc-BBN (**11**) conjugate. The images also reveal that the cell uptake of the RGD-peptide conjugate (**10**) is substantially lower as compared to that of the BBN analogue **11**, which likely reflects the higher hydrophilicity of the former (Figure 2).

CONCLUSION

The synthesis of a series of Pc-peptide conjugates was achieved via the solid-phase Sonogashira cross-coupling in moderate isolated yields for organo-soluble (~10–35%) and low to moderate yields for water-soluble analogues (~2–15%). Although the water-soluble conjugates were obtained in relatively low yields using solid-phase strategy, they were successfully prepared in rather high yields using an alternative approach, which also works well for organo-soluble analogues. In this approach, an iodinated water-soluble ZnPc was allowed to react with acetylenic model tripeptide and unprotected bombesin in solution to give corresponding conjugates in 70 and 50% isolated yields, compared to **11** and 2%, respectively, when using SPOS. The ZnPc-RGD conjugate **10** showed receptor binding character in photodynamic activity in vitro blocking studies, whereas its PDT efficacy was rather low, which could possibly be improved by conjugating the ZnPc to multimeric RGD peptide. Thus it has been shown that receptor binding characteristics of dimeric and multimeric RGD peptides are more advantageous than those of the monomeric RGD peptide.^{57,58} In the case of the water-soluble ZnPc-BBN

conjugate **11**, our data show its potential to function as both a fluorescence imaging probe and receptor-targeting photo-dynamic agent. These results warrant further *in vivo* studies to evaluate the potential of the *Pc*-bombesin conjugate for PDT of prostate, breast, and lung cancer that overexpress these receptors. Also, selective localization in these tumors would render the conjugates good candidates for PET imaging via substitution of the central Zn ion for positron emitting ^{64}Cu or ^{67}Cu isotopes.⁵⁹

EXPERIMENTAL SECTION

Synthesis. General Procedures. Unless otherwise stated, all reactions were carried out under argon atmosphere. All chemicals and solvents were used as supplied without further purification. ^1H and ^{13}C NMR spectra were recorded on a Bruker Spectrospin 300 instrument in $\text{DMSO-}d_6$ with the chemical shifts reported as δ in ppm and coupling constants expressed in Hz. The following abbreviations were used to describe spin multiplicity: s = singlet, d = doublet, t = triplet, q = quintet, dd = doublet of doublets, m = multiplet. LC-electrospray ionization (ESI⁺) mass spectra of the peptides were obtained with a Waters Micromass ZQ single-quadrupole mass spectrometer. MALDI-TOF mass spectra of the phthalocyanines (*Pc*), and the *Pc*-peptide conjugates were acquired in linear mode using a Micromass ToF Spec2E spectrometer, with α -cyano-4-hydroxycinnamic acid as the matrix (positive mode). Visible absorption spectra were recorded with Beckman DU 530 spectrophotometer. Analytical reverse-phase HPLC of the peptides **2a–2c**, **12a**, and **12b**, the water-soluble *Pc* **1c** and **13–16**, and *Pc*-peptide conjugates **9–11** was performed on an Agilent 1200 system equipped with an Agilent Eclipse XDB-C18 reverse phase column (4.6 mm \times 250 mm, 5 μ) and an Agilent 1200 series diode array UV/vis detector at a flow rate of 1 mL/min. Linear gradient of 0–100% acetonitrile in water (0.05% TFA) over 30 min was used for the peptides, whereas a linear gradient of 0–100% MeOH in phosphate buffer (10 mM, pH 5.0) over 40 min was employed for sulfonated *Pc*-peptide conjugates. Analytical reverse-phase HPLC of *tert*-butyl substituted *Pc* **1a–1b** and *Pc*-peptide conjugates **3–8** was carried out on a Hewlett-Packard 1050 system equipped with a Phenomenex Luna C18 reverse phase column (10 mm \times 250 mm, 5 μ) at a flow rate of 2 mL/min using isocratic elution with 65% aqueous THF as a mobile phase. Purification of peptides **12a** and **12b** was performed on the Hewlett-Packard 1050 system equipped with the Phenomenex Luna C18 semipreparative reverse phase column (10 mm \times 250 mm, 5 μ) at a flow rate of 2 mL/min using linear gradient of 20–100% acetonitrile in water with 0.05% TFA in 30 min. Conjugates **3–11** were purified via two-step semipreparative reverse phase HPLC on the Hewlett-Packard 1050 system equipped with the Phenomenex Luna C18 reverse phase column (10 mm \times 250 mm, 5 μ) at a flow rate of 2 mL/min. Linear gradient of 0–100% acetonitrile in water with 0.05% TFA in 20 min was first employed in order to eliminate peptides (*Pc*-peptide conjugates are not eluted in these conditions) followed by isocratic elution with THF for *tert*-butyl substituted *Pc*-peptide conjugates **3–8** or a linear gradient of 0–100% MeOH in phosphate buffer (10 mM, pH 5.0) in 40 min for sulfonated conjugates **9–11**. Silica gel column chromatography was carried out using 40–63 μm silica gel. All tested compounds were purified until at least 95% purity as judged by reverse phase HPLC. The identity of all the new compounds was confirmed by MALDI-TOF or ESI mass-spectrometry, UV-vis spectroscopy, as well as by ^1H and ^{13}C NMR for tripeptide **2a**.

Peptides Functionalized with Terminal Triple Bond. All peptides were synthesized manually using the Fmoc (fluorenylmethyloxycarbonyl) strategy and NovaSyn TGR resin. A 2.5-fold excess of Fmoc-protected amino acids over resin substitution rate was utilized for coupling. The amino acids were activated with an equimolar amount of HATU (2-(1*H*-7-azabenzotriazol-1-yl)-1,1,3,3-tetramethyluronium hexafluorophosphate) and 2-fold excess of *N,N*-diisopropylethylamine (DIPEA). After each coupling step, Fmoc deprotection was performed

in 20% piperidine in dimethylformamide (DMF). At the final step, 6-heptynoic acid was introduced at the N-terminal position after peptide assembly. The on-bead acetylenic peptides **2a–2c** thus obtained were used directly for the solid-phase Sonogashira cross-coupling with the iodinated phthalocyanines **1a–1c**. Purities of the resin-bound peptides were assessed by analytical reverse-phase HPLC after cleavage of \sim 10 mg of corresponding resin with the same cleavage cocktail, and their identities were confirmed using ESI mass spectrometry.

In parallel, the resin-bound **2a** and **2c** were treated with a cocktail of TFA:H₂O:thioanisole (92:2:6, v/v/v) at room temperature for 3 h to afford unprotected acetylenic peptides **12a** and **12b**, respectively. The crude peptides **12a** and **12b** were precipitated with cold diethyl ether (Et₂O) and then purified via reverse-phase HPLC on a semipreparative C18 column using a linear gradient of 20–100% acetonitrile in water with 0.05% TFA in 30 min. The isolated peptides **12a** and **12b** were then freeze-dried and stored at -20°C . Their purities were found to be >95% (analytical reverse-phase HPLC), and their structures were confirmed by ESI mass spectrometry as well as by ^1H and ^{13}C NMR for tripeptide **12a**.

Synthesis of Iodinated Phthalocyanines. Monoiodo *tri-tert*-Bu-ZnPc **1a**¹ and monoiodo trisulfonated ZnPc **1c**² were prepared following previously described procedures. The trisulfonated metal-free analogue **1b** was prepared from **1a** using a recently reported demetalation procedure³ for ZnPc. Zinc phthalocyanine **1a** (50 mg, 0.06 mmol) was stirred in pyridine (5 mL), and pyridine-HCl (1.5 g) under argon at 110°C for 17 h. After evaporation of the volatiles, the dark-green residue was redissolved in dichloromethane and extracted three times with water to remove pyridinium chloride salt. Then organic fraction was dried over anhydrous magnesium sulfate, filtered, and concentrated *in vacuo*. The resulting dark-blue residue was further purified by passing it down a short silica gel column (elution with 10% dioxane in hexane). The appropriate fraction was pooled and freed of solvent under reduced pressure to furnish the pure **1b** as dark-blue crystals (40 mg, 81%). HPLC profiles of the starting *Pc* and the *Pc*-peptide conjugates comprised of several peaks representing structural isomers because the statistical condensation route was used to obtain monoiodinated unsymmetrical zinc phthalocyanines **1a** and **1c**.

General Procedure for Sonogashira Cross-Coupling of Solid-Supported Acetylenic Peptides and Iodinated *Pc*. A reaction vial was charged with a solid-supported acetylenic peptide (25.0 mg, assumed \sim 0.24 mmol g⁻¹), Pd(OAc)₂ (0.34 mg, 50 mol %), (*o*-tolyl)₃P (1.18 mg, 150 mol %), and an iodinated phthalocyanine (0.003 mmol). Then the reaction vial was evacuated and purged with argon three times. Subsequently, 300 μL of degassed DMF was added under argon, followed by addition of DIPEA (8 μL , 15 equiv) degassed beforehand by gentle bubbling Ar through it for 30 min. After that, the reaction vial was tightly sealed and the resulting suspension was shaken at room temperature for 2 d in the case of conjugates **3–8** or gently stirred at 80°C for 1 d in the case of conjugates **9–11**. After cooling, the resin was separated by filtration and washed with DMF (3 \times 5 mL) and/or THF (3 \times 5 mL), CH₂Cl₂ (3 \times 5 mL), and MeOH (3 \times 5 mL) until the filtrate runs through colorless. The resin was then dried and treated with TFA-thioanisole-H₂O (92:6:2 v/v/v) for 4 h. Following filtration, the crude product was precipitated with Et₂O. The resulting solid was purified via two-step semipreparative RP-HPLC: at first the unreacted peptide and/or peptide homodimer was eluted with a 0–100% linear gradient of CH₃CN in water (containing 0.05% TFA) in 20 min while *Pc*-peptide conjugates were not eluted under these conditions. Afterward the *tert*-butyl substituted *Pc*-peptide conjugate **3–8** were eluted with THF while sulfonated *Pc*-peptide conjugates **9–11** were eluted with a linear gradient of 0–100% MeOH in phosphate buffer (10 mM, pH 5.0) in 40 min.

General Procedure for Sonogashira Cross-Coupling of Unprotected Acetylenic Peptides and Iodinated *Pcs* in Solution. Pd(OAc)₂ (0.68 mg, 50 mol %), (*o*-tolyl)₃P (2.36 mg, 150 mol %), an iodinated phthalocyanine (0.006 mmol), and an acetylenic unprotected peptide (0.009 mmol, 1.5-fold excess) were assembled in a round-bottomed flask sealed with a septum. The reaction flask was evacuated and purged with argon three times. Subsequently, 500 μL of degassed DMF was added under argon, followed by addition of DIPEA (16 μL ,

15 equiv) degassed beforehand by gentle bubbling Ar through it for 30 min. The reaction mixture was stirred at 70 °C until RP-HPLC showed complete conversion (0.5–1 h). The solvent was evaporated and the crude product was purified via two-step semipreparative RP-HPLC as described above.

Reference Phthalocyanines. ZnPc **13** was prepared from ZnPc **1c** under the copper-free Sonogashira cross-coupling conditions. **1c** (40 mg, 0.04 mmol) was reacted with 5-fold excess of 5-hexynoic acid (22 mg, 0.2 mmol) in the presence of 50 mol % Pd(OAc)₂ (4.4 mg, 0.02 mmol)/100 mol % (*o*-tolyl)₃P (12.2 mg, 0.04 mmol) and 15 equiv of DIPEA (0.6 mmol, 104 μL) in anhydrous DMF (3 mL) at 70 °C overnight. Then solvent was evaporated under reduced pressure, the residue was redissolved in minimal amount of water, and *Pc* was precipitated by adding an excess of ethanol. The blue precipitate was filtered off, washed on the filter with ethanol, and dried to give the desired product **13** as dark-blue powder (29 mg, 73%). The structures of **1b** and **13** were confirmed by MALDI-TOF mass-spectrometry and UV–vis spectroscopy. The purity of **13** was estimated by analytical HPLC on a C18 reverse phase column using a linear gradient of 0–100% MeOH in phosphate buffer (5 mM, pH 5.0) in 40 min and found to be greater than 95%. MALDI-TOF MS (*m/z*): [M⁺] calcd for C₃₈H₂₂N₈O₁₁S₃Zn, 928.23, found 928.47; UV–vis λ_{max} (DMF): 680, 613 (sh), 354; HPLC (676 nm): three close peaks, *t*_R 27.8–30.2 min. Three other reference compounds, e.g., ZnPcS₂ (**14**), ZnPcS₃ (**15**),⁴ and ZnPcS₃C₆ (**16**)² were prepared as previously described.

Biology. Cell Cultures. All cell lines were purchased from American Type Culture Collection (ATCC, Manassas, VA, USA) and maintained in T75 flasks (Falcon, Mississauga, Canada) in specific media at 37 °C, under 5% CO₂ and 95% air. All culture media were supplemented with 1% L-glutamine, 1% penicillin–streptomycin (GIBCO, Burlington, Canada). The cell lines used in these studies include the murine mammary EMT-6 (ATCC CRL-2755), human breast adenocarcinoma MDA-MB-231 (ATCC HTB-26), human lung adenocarcinoma A549 (ATCC CCL-185), and human prostate cancer PC3 (ATCC CRL-1435). EMT-6 cells were maintained in Waymouth MB 752/1 medium fortified with 15% fetal bovine serum (FBS), MDA-MB-231 cells in EMEM with 10% FBS, A549 in RPMI 1640 with 10% fetal calf serum, and PC3 in HAM F12K with 10% fetal calf serum. The cells were transferred periodically following treatment with trypsin (0.05%).

Western Blot Analysis.⁶⁰ The relative concentrations of integrin and GRP receptors in the cell lines were established by Western blot analysis. Briefly, cells were washed with PBS (3 times) and total protein was extracted (10 mM Tris base-HCl, 150 mM NaCl, 1% NP-40, 1% Triton X-100, 5 mM EDTA, 0.1% SDS, 1% sodium deoxycholate, 1 mM phenylmethylsulfonyl fluoride, 1 μg/mL aprotinin, 1 μg/mL pepstatin, 1 μg/mL leupeptin, 1% sodium orthovanadate, and 50 mM sodium fluoride). Cellular debris was cleared by centrifugation, and supernatants (lysates) were aliquoted and stored at –20 °C. The concentration of lysates was determined by the Bradford method (Bio-Rad protein assay).⁶¹ Briefly, the protein extracts were applied on a 4–20% mini-protein TGX Stain Free Precast gels at 160 V during 1 h and transferred to a PVDF membrane (Millipore, Bedford, MA, USA) using the Mini Trans-Blot Cell (Bio-Rad) settled at 100 V for 1 h. In all cases, the membrane was blocked during 2 h at room temperature with 5% reconstituted skim milk powder in TBST solution (10 mM Tris-HCl pH 7.5 containing 150 mM NaCl and 0.05% Tween 20). Membranes were incubated overnight at 4 °C under continuous agitation with primary antibodies β-actin, sc-47778, integrin α₃, sc-374242 and GRPR(F6), SC377316 (Santa Cruz Biotechnology, CA, USA), integrin α_vβ₃, MAB 1961 (Millipore, MA, USA), and integrin α_vβ₃, CD61 (Biosciences, ON, Canada) and washed 3 times with TBS-T. Then they were incubated with secondary antibodies goat antimouse IgG-HRP, sc-2005 (Santa Cruz Biotechnology, CA, USA) for 2 h at room temperature. Detection of immunoreactive bands was performed using the enhanced chemiluminescence (Plus-ECL) detection kit (PerkinElmer Inc., MA, USA).⁶² The protein levels that corresponded to the immunoreactive bands were quantified using the Image J analysis

software (Wayne Rasband, NIH, USA). The protein intensity was determinate by intensity multiply by protein band area.

Cellular Uptake. Tumor cells (1.5 × 10⁵ cells per well) in 1 mL of their specific growth medium were incubated in 24-well plates (Falcon) overnight at 37 °C under 5% CO₂. The medium was removed, and the monolayer was rinsed twice with 1% PBS and then overlaid with 500 μL of the dye solution (2 μM) in a combination medium prepared from equal amounts of the four specific growth media supplemented with 4% FBS. After 24 h incubation, the dye solution was removed and the cells were washed twice with 1% PBS. The cells were lysed with 500 μL of 0.1 N NaOH. An aliquot (50 μL) was removed to determine cellular protein according to the Bradford method (Bio-Rad protein assay).⁶¹ DMF (450 μL) and 1% PBS (100 μL) were added to the remaining cell lysate, the mixture was centrifuged for 30 min at 4 °C, 3500 rpm, and dye concentration in the clear supernatant was assayed by fluorescence spectroscopy (F-2000, Hitachi) (λ_{ex} 608 nm, 5 nm band-pass, λ_{em} 680 nm, 10 nm band-pass). Standard curves were obtained using cell lysates treated as above with known amounts of the appropriate *Pc* solution. The cellular ZnPc concentration is expressed as nmole of *Pc* per mg of cellular protein.

Cell Photoinactivation. Cell cultures were trypsinated to give a 1.5 × 10⁵ cells/mL suspension of which 100 μL per well were plated in 96-well plates and incubated overnight at 37 °C under 5% CO₂. Attached cells were rinsed twice with PBS and incubated for 24 h with 50 μL of dye solution (2 μM) in a combination medium prepared from equal amounts of the four specific growth media supplemented with 4% FBS. One column did not receive cells to serve as a blank, while a second control column was filled with dye-free medium only. The cells were then rinsed twice with PBS, reseeded with 100 μL of specific culture medium, and exposed for varying time intervals to red light (10 mW·cm⁻² at 660–700 nm). For illumination, we used a homemade device consisting of two 500 W tungsten–halogen lamps fitted with an aqueous rhodamine B (OD₅₈₀ = 1.25) (Sigma, Canada) filter connected to a cold water bath. The emitted light intensity was calibrated by a photometer (model LI-185B, LI-COR Biosciences inc. Nebraska USA). Plates were incubated overnight at 37 °C under 5% CO₂. Cell survival was measured by a colorimetric method, using the tetrazolium salt MTT (3-(4,5-dimethylthiazol-2-yl)-2,5-diphenyltetrazolium bromide) (Sigma). Eight replicates were run, and experiments were repeated at least three times. The survival curves were plotted as a function of light dose and LD₅₀ values were calculated.

PDT-Inhibition with BBN and RGD. PDT-inhibition assays were performed on all four tumor cell lines detailed in the cell culture section. Cell cultures were trypsinated to give a 1.5 × 10⁵ cells/mL suspension, of which 100 μL per well were incubated in 96-well plates overnight at 37 °C under 5% CO₂. Attached cells were rinsed twice with PBS and incubated for 24 h with 50 μL of 2 μM ZnPc–RGD (**10**) or ZnPc–BBN (**11**) in a mixture of the four culture media (25% each), supplemented with 4% FBS. One row did not receive cells to serve as a blank, while a second control row was filled with dye-free medium only. Two hours before PS addition, the other rows received 50 μL/well of BBN or RGD in increasing concentrations from 10⁻¹² to 10⁻⁵ M. The plates were incubated for 24 h at 37 °C, where after the incubation medium was removed, cells were washed three times with PBS, reseeded with 100 μL of specific culture medium, and exposed for 20 min to red light (10 mW·cm⁻², 12 J·cm⁻², at 660–700 nm). Plates were incubated overnight at 37 °C under 5% CO₂. Cell survival was measured by the MTT test. Eight replicates were run, and experiments were repeated at least three times. Finally, data were analyzed with GraphPad Prism 5 software to determine the IC₅₀ value, e.g., the BBN or RGD concentration required to reduce the PDT response by 50%. A similar PDT inhibition protocol was used to determine the effect of BBN on 2 μM nonconjugated ZnPc (**13**–**16**). To allow a significant PDT response, inhibitor concentration (BBN or RGD) and light dose were fixed at 1 nM and 12 J·cm⁻², respectively.

Intracellular Distribution. The PC3 and MDA-MB-231 cell suspensions (10⁴ cells/mL) were plated onto 12 mm diameter glass coverslips (Fisher Scientific) placed in 24-well plates and incubated for 18–24 h at 37 °C, under 5% CO₂, to allow for cell adhesion. The medium was removed, and the cells were rinsed twice with PBS and

then overlaid with 0.1 mL of the ZnPc-peptide solution (10 μ M) in their specific medium culture supplemented with 1% FBS. After 18 h at 37 °C, the solution was removed and cells were washed twice with PBS and twice with HBSS/HEPES buffer. The cells were incubated at 37 °C under 5% CO₂ with different tracker dyes (Invitrogen Inc., Ontario, Canada) including Myto-Tracker green (150 nM, 45 min), Lyso-Tracker Green (200 nM, 1 h), TMA-DPH or 1-[4-(methylamino)phenyl]-6-phenylhexa-1,3,5-triene (5 μ M, 1 h), and NBDC6 Ceramide (5 μ M, 1 h). Only the latter dye needed to be rinsed three times, after which the cells were incubated for another 30 min. After the last incubation, all samples were washed twice with PBS. For TMA-DPH staining, with and without ZnPc-peptide conjugates (10 and 11), slides were mounted for microscopic observations using Vectashield mounting media (Vector Laboratories, Peterborough, U.K.). The Vectashield including DAPI mounting media (Vector Laboratories, Peterborough, U.K.) was used for all other staining.

For blocking studies, PC3 and MDA-MB-231 suspensions (10⁴ cells/mL) were plated onto 12 mm diameter glass coverslips (Fisher Scientific) placed in 24-well plates and incubated for 18–24 h at 37 °C, under 5% CO₂, to allow for cell adhesion. The medium was removed, and the cells were rinsed twice with PBS and then overlaid with 0.1 mL of new specific culture medium, with or without 1 nM final concentration of specific inhibitor (BBN or RGD). After 2 h, the medium was removed, and the cells were rinsed twice with PBS and then replaced by 0.1 mL of ZnPc-RGD (10) or ZnPc-BBN (11) (10 μ M), or their specific medium culture alone, supplemented with 1% FBS in the corresponding well (e.g., BBN, RGD, or blank). After 18 h at 37 °C, the solution was removed and the cells were washed twice with PBS and twice more with HBSS/HEPES buffer. The cells were mounted for microscopic observations with Vectashield mounting medium.

Confocal Microscopic Analysis. Cells were examined with a scanning confocal microscope (FV1000, Olympus, Tokyo, Japan) coupled to an inverted microscope with a 63 \times oil immersion objective (Olympus). Specimens were laser-excited at 405 nm (DAPI and TMA-DPH), 488 nm (Myto-Tracker green, Lyso-Tracker Green and NBDC6 Ceramide), or 633 nm (ZnPc), and the fluorescence was collected with FL1 (blue, 440–470 nm), FL2 (green, 500–530 nm), and FL3 (red, >640 nm), respectively. Serial horizontal optical sections of 512 \times 512 pixels with two times line averaging were taken at 0.4 μ m intervals through the entire thickness of the cell (optical resolution: lateral –0.2 μ m, axial –0.8 μ m). Images were acquired during the same day, typically from five cells of similar size, from each experimental condition using identical settings of the instrument. For merged fluorescence images the dots fluorograms were obtained by plotting pixel values of each component toward horizontal and vertical axis, respectively. Quadrant markers were placed forming background (C), red-only (D), green-only (A), and colocalization areas (B). Colocalization index were calculated as (B)/(B + D), and % of colocalization as (B)/(B + D) \times 100.⁶³ Quantitative analysis was performed on five size-matched cells for each experimental condition, and experiments were performed three times. For illustration purposes, images were contrast enhanced, pseudocolored accordingly to their original fluorochromes, merged (FluoView software, Olympus), and then cropped and assembled (Adobe Photoshop software, Mountain View, CA).

■ ASSOCIATED CONTENT

● Supporting Information

General synthetic procedures and analytical data for **1b**, **13**, **2a–2c**, **3–11**, **12a**, and **12b**, including copies of the ¹H NMR, ¹³C NMR, UV–vis, MALDI-TOF, ESI-MS spectra, and HPLC traces, cell survival curves, and Western blots. This material is available free of charge via the Internet at <http://pubs.acs.org>.

■ AUTHOR INFORMATION

Corresponding Author

*Phone: +1 819 564 5409. E-mail: Johan.E.vanLier@USherbrooke.ca (J.E.v.L.); Brigitte.Guerin2@USherbrooke.ca (B.G.).

Notes

The authors declare no competing financial interest.

■ ACKNOWLEDGMENTS

J.E.v.L. and B.G. are members of the Fonds de la Recherche en Santé du Québec-supported CRC Étienne-Le Bel of the Centre Hospitalier Universitaire de Sherbrooke, Sherbrooke, QC, Canada. This work was supported by an NSERC Strategic Projects Grant (Canada) and the Jeanne and J.-Louis Lévesque Chair in Radiobiology.

■ ABBREVIATIONS USED

PDT, photodynamic therapy; BBN, bombesin; GRP, gastrin-releasing peptide; GRPR, gastrin-releasing peptide receptor; RGD, arginine–glycine–aspartic acid, integrin binding motif; YVG, tyrosine–valine–glycine, nonspecific peptide; $\alpha_v\beta_3$, RGD binding integrin; $\alpha_v\beta_5$, RGD binding integrin; mAbs, monoclonal antibodies; PS, photosensitizer; Pc, phthalocyanines; PcS, sulfonated phthalocyanines; Fmoc, fluorenylmethoxycarbonyl; LD₅₀, fluence required for 50% cell survival; IC₅₀, BBN or RGD concentration required for 50% inhibition of PDT response; SPOS, solid-phase organic synthesis

■ REFERENCES

- (1) Celli, J. P.; Spring, B. Q.; Rizvi, I.; Evans, C. L.; Samkoe, K. S.; Verma, S.; Pogue, B. W.; Hasan, T. Imaging and photodynamic therapy: mechanisms, monitoring, and optimization. *Chem. Rev.* **2010**, *110*, 2795–2838.
- (2) Lovell, J. F.; Liu, T. W.; Chen, J.; Zheng, G. Activatable photosensitizers for imaging and therapy. *Chem. Rev.* **2010**, *110*, 2839–2857.
- (3) Ethirajan, M.; Chen, Y.; Joshi, P.; Pandey, R. K. The role of porphyrin chemistry in tumor imaging and photodynamic therapy. *Chem. Soc. Rev.* **2011**, *40*, 340–362.
- (4) Wilson, B. C.; Patterson, M. S. The physics, biophysics and technology of photodynamic therapy. *Phys. Med. Biol.* **2008**, *53*, R61–109.
- (5) Ali, H.; van Lier, J. E. Metal complexes as photo- and radiosensitizers. *Chem. Rev.* **1999**, *99*, 2379–2450.
- (6) Ali, H.; van Lier, J. E. Porphyrins and phthalocyanines as photo- and radiosensitizers. In *Handbook of Porphyrin Science: Phototherapy, Radioimmunotherapy and Imaging*; Kadish, K. M., Smith, K. M., Guillard, R., Eds.; World Scientific Publishing: Hackensack, NJ, 2010; Vol. 4, pp 1–120.
- (7) Shinohara, H.; Tsaryova, O.; Schnurpfeil, G.; Wohrle, D. Differently substituted phthalocyanines: comparison of calculated energy levels, singlet oxygen quantum yields, photo-oxidative stabilities, photocatalytic and catalytic activities. *J. Photochem. Photobiol., A* **2006**, *184*, 50–57.
- (8) Brozek-Pluska, B.; Jarota, A.; Jablonska-Gajewicz, J.; Kordek, R.; Czajkowski, W.; Abramczyk, H. Distribution of phthalocyanines and raman reporters in human cancerous and noncancerous breast tissue as studied by raman imaging. *Technol. Cancer Res. Treat.* **2012**, *4*, 301–408.
- (9) Kudrevich, S.; Brasseur, N.; La Madeleine, C.; Gilbert, S.; van Lier, J. E. Syntheses and photodynamic activities of novel trisulfonated zinc phthalocyanine derivatives. *J. Med. Chem.* **1997**, *40*, 3897–3904.
- (10) Cauchon, N.; Tian, H.; Langlois, R.; La Madeleine, C.; Martin, S.; Ali, H.; Hunting, D.; van Lier, J. E. Structure–photodynamic

activity relationships of substituted zinc trisulfophthalocyanines. *Bioconjugate Chem.* **2005**, *16*, 80–89.

(11) Sharman, W. M.; van Lier, J. E.; Allen, C. M. Targeted photodynamic therapy via receptor mediated delivery systems. *Adv. Drug Delivery Rev.* **2004**, *56*, 53–77.

(12) Shadidi, M.; Sioud, M. Selective targeting of cancer cells using synthetic peptides. *Drug Resist. Update* **2003**, *6*, 363–371.

(13) Gentilucci, L.; De Marco, R.; Cerisoll, L. Chemical modifications designed to improve peptide stability: incorporation of non-natural amino acids, pseudo-peptide bonds, and cyclization. *Curr. Pharm. Des.* **2010**, *16*, 3185–3203.

(14) Xiao, D.; Wang, J.; Hampton, L. L.; Weber, H. C. The human gastrin-releasing peptide receptor gene structure, its tissue expression and promoter. *Gene* **2001**, *264*, 95–103.

(15) Plonowski, A.; Nagy, A.; Schally, A. V.; Sun, B.; Groot, K.; Halmos, G. In vivo inhibition of PC-3 human androgen-independent prostate cancer by a targeted cytotoxic bombesin analogue, AN-215. *Int. J. Cancer* **2000**, *88*, 652–657.

(16) Sancho, V.; Di Florio, A.; Moody, T. W.; Jensen, R. T. Bombesin receptor-mediated imaging and cytotoxicity: review and current status. *Curr. Drug Delivery* **2011**, *8*, 79–134.

(17) Craft, J. M.; De Silva, R. A.; Lears, K. A.; Andrews, R.; Liang, K.; Achilefu, S.; Rogers, B. E. In vitro and in vivo evaluation of a ⁶⁴Cu-labeled NOTA-Bn-SCN-Aoc-bombesin analogue in gastrin-releasing peptide receptor expressing prostate cancer. *Nuclear Med. Biol.* **2012**, *39*, 609–616.

(18) Fournier, P.; Dumulon-Perreault, V.; Ait-Mohand, S.; Tremblay, S.; Bénard, F.; Lecomte, R.; Guérin, B. Novel radiolabeled peptides for breast and prostate tumor PET imaging: ⁶⁴Cu/ and ⁶⁸Ga/NOTA-PEG-[D-Tyr6,βAla11,Thi13,Nle14]BBN(6–14). *Bioconjugate Chem.* **2012**, *3*, 1687–1693.

(19) Mantey, S. A.; Coy, D. H.; Entsuaeh, L. K.; Jensen, R. T. Development of bombesin analogs with conformationally restricted amino acid substitutions with enhanced selectivity for the orphan receptor human bombesin receptor subtype 3. *J. Pharmacol. Exp. Ther.* **2004**, *310*, 1161–1170.

(20) Plow, E. F.; Haas, T. A.; Zhang, L.; Loftus, J.; Smith, J. F. Ligand binding to integrins. *J. Biol. Chem.* **2000**, *275*, 21785–21788.

(21) Takagi, J. Structural basis for ligand recognition by RGD (Arg-Gly-asp)-dependent integrins. *Biochem. Soc. Trans.* **2004**, *32*, 402–406.

(22) Takada, Y.; Ye, X.; Simon, S. The integrins. *Genome Biol.* **2007**, *8* (5), 215.

(23) Arosio, D.; Manzoni, L.; Araldi, E. M. V.; Caprini, A.; Monferini, E.; Scolastico, C. Functionalized cyclic RGD peptidomimetics: conjugable ligands for αvβ3 receptor imaging. *Bioconjugate Chem.* **2009**, *20*, 1611–1617.

(24) Meyer, A.; Auernheimer, J.; Modlinger, A.; Kessler, H. Targeting RGD recognizing integrins: drug development, biomaterial research, tumor imaging and targeting. *Curr. Pharm. Des.* **2006**, *12*, 2723–2747.

(25) Avraamides, C. J.; Garmy-Susini, B.; Varner, J. A. Integrins in angiogenesis and lymphangiogenesis. *Nature Rev. Cancer* **2008**, *8*, 604–617.

(26) Dubuc, C.; Langlois, R.; Benard, F.; Cauchon, N.; Klarskov, K.; Tone, P.; van Lier, J. E. Targeting gastrin-releasing peptide receptors of prostate cancer cells for photodynamic therapy with a phthalocyanine–bombesin conjugate. *Bioorg. Med. Chem. Lett.* **2008**, *18*, 2424–2427.

(27) Sibrian-Vazquez, M.; Ortiz, J.; Nesterova, I. V.; Fernandez-Lazaro, F.; Sastre-Santos, A.; Soper, S. A.; Vicente, M. G. H. Synthesis and properties of cell-targeted Zn(II)-phthalocyanine–peptide conjugates. *Bioconjugate Chem.* **2007**, *18*, 410–420.

(28) Brasseur, N.; Langlois, R.; La Madeleine, C.; Ouellet, R.; van Lier, J. E. Receptor-mediated targeting of phthalocyanines to macrophages via covalent coupling to native or maleylated bovine serum albumin. *Photochem. Photobiol.* **1999**, *69*, 345–352.

(29) Mudyiwa, M.; Ndinguri, M. W.; Soper, S. A.; Hammer, R. P. Microwave assisted solid-phase synthesis of substituted tetraazaporphyrins and a phthalocyanine–peptide conjugate. *J. Porphyrins Phthalocyanines* **2010**, *14*, 891–903.

(30) Ali, H.; Ait-Mohand, S.; Gosselin, S.; van Lier, J. E.; Guerin, B. Phthalocyanine–peptide conjugates via palladium-catalyzed cross-coupling reactions. *J. Org. Chem.* **2011**, *76*, 1887–1890.

(31) Chinchilla, R.; Najera, C. Recent advances in Sonogashira reactions. *Chem. Soc. Rev.* **2011**, *40*, 5084–5121.

(32) Testero, S. A.; Mata, E. G. Prospect of metal-catalyzed C–C forming cross-coupling reactions in modern solid-phase organic synthesis. *J. Comb. Chem.* **2008**, *10*, 487–497.

(33) Spivey, A. C.; McKendrick, J.; Srikanan, R.; Helm, B. A. Solid-phase synthesis of an A–B loop mimetic of the Cepsilon3 domain of human IgE: macrocyclization by Sonogashira coupling. *J. Org. Chem.* **2003**, *68*, 1843–1851.

(34) Dyatkin, A. B.; Rivero, R. A. The solid phase synthesis of complex propargylamines using the combination of Sonogashira and Mannich reactions. *Tetrahedron Lett.* **1998**, *39*, 3647–3650.

(35) Evano, G.; Blanchard, N.; Toumi, M. Copper-mediated coupling reactions and their applications in natural products and designed biomolecules synthesis. *Chem. Rev.* **2008**, *108*, 3054–3131.

(36) Leikoski, T.; Kallonen, S.; Yli-Kauhaluoma, J. The Sonogashira coupling of polymer-supported propargylamine with aryl iodides. *Helv. Chim. Acta* **2010**, *93*, 39–47.

(37) Liang, B.; Dai, M.; Chen, J.; Yang, Z. Copper-free Sonogashira coupling reaction with PdCl₂ in water under aerobic conditions. *J. Org. Chem.* **2005**, *70*, 391–393.

(38) Hutchins, S. M.; Chapman, K. T. Fisher indole synthesis on a solid support. *Tetrahedron Lett.* **1996**, *37*, 4869–4872.

(39) Ali, H.; Langlois, R.; Wagner, J. R.; Brasseur, N.; Paquette, B.; van Lier, J. E. Biological activities of phthalocyanines. X. Syntheses and analyses of sulfonated phthalocyanines. *Photochem. Photobiol.* **1988**, *47*, 713–717.

(40) Dibowski, H.; Schmidtchen, F. P. Bioconjugation of peptides by palladium-catalyzed C–C cross-coupling in water. *Angew. Chem., Int. Ed.* **1998**, *37*, 476–478.

(41) Bong, D. T.; Ghadiri, M. R. Chemoselective Pd(0)-catalyzed peptide coupling in water. *Org. Lett.* **2001**, *3*, 2509–2511.

(42) Cho, J. H.; Prickett, C. D.; Shaughnessy, K. H. Efficient Sonogashira coupling of unprotected halonucleosides in aqueous solvents using water-soluble palladium catalysts. *Eur. J. Org. Chem.* **2010**, *19*, 3678–3683.

(43) Goodman, S. L.; Grote, H. J.; Wilm, C. Matched rabbit monoclonal antibodies against αv-series integrins reveal a novel αvβ3-LIBS epitope and permit routine staining of archival paraffin samples of human tumors. *Biol. Open* **2012**, *1*, 329–340.

(44) Wong, N. C.; Mueller, B. M.; Barbas, C. F.; Ruminski, P.; Quaranta, V.; Lin, E. C.; Smith, J. W. Alpha v integrins mediate adhesion and migration of breast carcinoma cell lines. *Clin. Exp. Metastasis* **1998**, *16*, 50–61.

(45) Meyer, T.; Marshall, J. F.; Hart, I. R. Expression of αv integrins and vitronectin receptor identity in breast cancer cells. *Br. J. Cancer* **1998**, *77*, 530–536.

(46) Liu, Z.; Yan, Y.; Liu, S.; Wang, F.; Chen, X. ¹⁸F, ⁶⁴Cu and ⁶⁸Ca labeled RGD–bombesin heterodimeric peptide for PET imaging of breast cancer. *Bioconjugate Chem.* **2009**, *20*, 1016–1025.

(47) Okarvi, S. M.; Jammaz, I. A. Preparation and evaluation of bombesin peptide derivatives as potential tumor imaging agents: effects of structure and composition of amino acid sequence on in vitro and in vivo characteristics. *Nucl. Med. Biol.* **2012**, *39*, 795–804.

(48) Siegfried, J. M.; Han, Y. H.; DeMichele, M. A.; Hunt, J. D.; Gaither, A. L.; Cuttitta, F. Production of gastrin-releasing peptide by a non-small cell lung carcinoma cell line adapted to serum-free and growth factor-free conditions. *J. Biol. Chem.* **1994**, *269*, 8596–8603.

(49) Jackson, A. B.; Nanda, P. K.; Rold, T. L.; Sieckman, G. L.; Szczodroski, A. F.; Hoffman, T. J.; Chen, X.; Smith, C. J. ⁶⁴Cu-NO₂A-RGD-Glu-6-Ahx-BBN(7–14)NH₂: a heterodimeric targeting vector for positron emission tomography imaging of prostate cancer. *Nucl. Med. Biol.* **2012**, *39*, 377–387.

(50) Liu, Z.; Li, Z.-B.; Cao, Q.; Liu, S.; Wang, F.; Chen, X. Small-animal PET of tumors with ^{64}Cu -labeled RGD–bombesin heterodimer. *J. Nucl. Med.* **2009**, *50*, 1168–1177.

(51) Bonaccorsi, L.; Carloni, V.; Muratori, M.; Salvadori, A.; Giannini, A.; Carini, M.; Serio, M.; Forti, G.; Baldi, E. Androgen receptor expression in prostate carcinoma cells suppresses $\alpha 6/\beta 4$ integrin-mediated invasive phenotype. *Endocrinology* **2000**, *141*, 3172–3182.

(52) Frochot, C.; Di Stasio, B.; Vanderesse, R.; Belgy, M. J.; Dodeller, M.; Guillemin, F.; Viriot, M. L.; Barberi-Heyob, M. Interest of RGD-containing linear or cyclic peptide targeted tetraphenyl-chlorin as novel photosensitizers for selective photodynamic activity. *Bioorg. Chem.* **2007**, *35*, 205–220.

(53) Allen, C. M.; Sharman, W. M.; La Madeleine, C.; van Lier, J. E.; Weber, J. M. Attenuation of photodynamically induced apoptosis by an RGD containing peptide. *Photochem. Photobiol. Sci.* **2002**, *1*, 246–254.

(54) McQuade, P.; Knight, L. C.; Welch, M. J. Evaluation of ^{64}Cu - and ^{125}I -radiolabeled bitistatin as potential agents for targeting alpha v beta 3 integrins in tumor angiogenesis. *Bioconjugate Chem.* **2004**, *15*, 988–996.

(55) Pogue, B. W.; Redmond, R. W.; Trivedi, N.; Hasan, T. Photophysical properties of tin ethyl etiopurpurin I (SnET) and tin octaethylbenzochlorin (SnOEBC) in solution and bound to albumin. *Photochem. Photobiol.* **1998**, *68*, 809–815.

(56) Guojun, W.; Wei, G.; Kedong, O.; Yi, H.; Yanfei, X.; Qingmei, C.; Yankai, Z.; Jie, W.; Hao, F.; Taiming, L.; Jingjing, L.; Rongyue, C. A novel vaccine targeting gastrin-releasing peptide: efficient inhibition of breast cancer growth in vivo. *Endocr.-Relat. Cancer* **2008**, *15*, 149–159.

(57) Liu, Z.; Wang, F.; Chen, X. Integrin targeted delivery of radiotherapeutics. *Theranostics* **2011**, *1*, 201–210.

(58) Liu, Z.; Niu, G.; Wang, F.; Chen, X. ^{68}Ga -labeled NOTA-RGD-BBN peptide for dual integrin and GRPR-targeted tumor imaging. *Eur. J. Nucl. Med. Mol. Imaging* **2009**, *36*, 1483–1494.

(59) Ranyuk, E. R.; Cauchon, N.; Ali, H.; Lecomte, R.; Guérin, B.; van Lier, J. E. PET imaging using ^{64}Cu -labeled sulfophthalocyanines: synthesis and biodistribution. *Bioorg. Med. Chem. Lett.* **2011**, *21*, 7470–7473.

(60) Gilbert, C.; Rollet-Labelle, E.; Caon, A. C.; Naccache, P. H. Immunoblotting and sequential lysis protocols for the analysis of tyrosine phosphorylation-dependent signaling. *J. Immunol. Methods* **2002**, *271*, 185–201.

(61) Bradford, M. M. A rapid and sensitive method for the quantitation of microgram quantities of protein utilizing the principle of protein–dye binding. *Anal. Biochem.* **1976**, *72*, 248–254.

(62) Thorpe, G. H. G.; Kricka, L. J.; Mosely, S. B.; Whitehead, T. P. Phenols as enhancers of the chemiluminescent horseradish peroxidase–luminal–hydrogen peroxide reaction: application in luminescence-monitored enzyme immunoassays. *Clin. Chem.* **1985**, *31*, 1335–1341.

(63) Manders, E. M. M.; Verbeek, F. J.; Aten, J. A. Measurement of colocalization of objects in dual-color confocal images. *J. Microsc.* **1993**, *169*, 375–382.